Anatomically modern human dispersals into Europe during MIS 3: Climate stability, paleogeography and habitat suitability

Simon Paquin, Benjamin Albouy, Masa Kageyama, Mathieu Vrac, Ariane Burke

Anatomically Modern Human dispersals into Europe during MIS 3: climate stability, paleogeography and habitat suitability.

Simon Paquin[1], Benjamin Albouy[1], Masa Kageyama[2], Mathieu Vrac[2] & Ariane Burke[1]

[1]Département d'anthropologie, Université de Montréal
Pavillon Lionel-Groulx, 3150 Jean-Brillant, Montréal, QC, H3T 1N8, Canada
(simon.paquin@umontreal.ca)* Corresponding author
(benjamin.albouy@umontreal.ca)
(a.burke@umontreal.ca)

[2]Laboratoire des Sciences du Climat et de l'Environnement (LSCE-IPSL),
Centre d'Études de Saclay, Orme des Merisiers, Bat. 714, 91191 Gif-sur-Yvette, France
(masa.kageyama@lsce.ipsl.fr)
(Mathieu.vrac@lsce.ipsl.fr)

Keywords: Aurignacian technocomplex, MIS3, Habitat Suitability, Climate Change, Paleogeography, Human dispersal, Europe

Abstract: The initial large-scale dispersal of Anatomically Modern Humans (AMHs) into Europe, associated with the Aurignacian technocomplex, occurred during Marine Isotope Stage 3 (MIS 3), a critically unstable climatic period. The impact of climate change (millennial-scale Dansgaard-Oeschger events) and climate variability (annual and seasonal variation) on the mobility and initial dispersal of AMHs on the continent is not fully demonstrated. Here we show that both climate change and variability affected the spatial behavior of Aurignacian groups and structured their arrival on the continent. Using Random Forest, a machine learning algorithm, we produced habitat suitability (HS) models for AMHs under stadial (GS) and interstadial (GI) climate conditions. These models demonstrate that climate variability was a key factor governing the spatial behavior of human groups across MIS 3. They also illustrate that the structure and distribution of suitable habitat in Europe were affected by climatic conditions, with implications in terms of our species' adaptability and behavioral plasticity. Finally, our results support the suggestion that initial dispersals followed a Mediterranean coastal route, likely under interstadial conditions.

1 Introduction

Dispersal events are a defining feature of human history and adaptation. As our species, *Homo sapiens*, spread into new landscapes during the Late Pleistocene it faced a variety of new and challenging situations, including coexistence with other human groups such as the Neanderthals and Denisovans, and novel and at times rapidly changing

environmental contexts. Dispersals may also act as triggers for the biological evolution of the genus Homo (Timmermann et al., 2022). Of particular interest here is the dispersal of Aurignacian populations into Europe during Marine Isotopic Stage 3 (MIS 3) possibly following initial AMHs entry circa. 55,000 years go (55 ka) (Slimak et al., 2022). Despite the documented climate instability of MIS 3 AMHs successfully settled the European continent while Neanderthal populations declined (Banks et al., 2013a, 2013b, 2008; d'Errico and Sánchez Goñi, 2003; Gamble et al., 2004; Higham et al., 2014; Hublin, 2015; Klein et al. 2023; Mellars, 2006, 2011; Müller et al., 2011; Paquin et al., 2023; Timmermann, 2020; Tzedakis et al., 2007; Zilhão and d'Errico, 1999). This is obviously a condensed outline of a far more complex process for which scientific investigation is incomplete. Environmental change, landscape transformation and human dispersal interconnect and play out over long-time scales, determining the course of human evolution. The relationship between these variables is central to understanding the Paleolithic period, and especially crucial when comparing the fate of different human groups. The main goal of this research is to better understand the impact of millennial-scale climate variation and climate instability on the pattern of dispersal of AMHs into Europe during MIS3.

Computational archaeology has come a long way since the 20th century and modelling techniques are now widely used for studying human/environment interactions (e.g., Banks et al., 2008, 2013a; Burke et al., 2014, 2017; Klein et al., 2021, 2023; Ludwig et al., 2018; Maier et al., 2016; Schmidt et al., 2012; Shao et al., 2021; Tallavaara et al., 2015; Timmermann, 2020; Tsakanikou & McNabb, 2023; Weniger et al., 2019). We use HS modelling to define and map the distribution of suitable habitat for Aurignacian groups

entering Europe during MIS 3 stadial (GS) and interstadial (GI) events. Comparing the HS models allows us to measure the impact of these contrasting climate events on the distribution of AMH populations. As part of the modelling process, we also identify key environmental variables to which AMHs responded during MIS 3.

1.1 Climate change and Dispersal

Mobility is a central component of the human adaptative system. Multiple dispersal events have occurred since the evolution of our species in Africa. Uncovering the environmental parameters that facilitated or hindered these phenomena is instrumental to understanding them. The initial AMH dispersal into the Levant from Africa *ca.* 200-120 Kyr BP is hypothetically linked to a geographical extension of their habitat, composed of riverine woodlands or grasslands, during interstadial cycles (Hershkovitz et al., 2018; Vaks et al., 2007). Later dispersal events out of the African continent *ca*. 60-50 ka BP are also hypothetically linked to the development of humid climates in the eastern Mediterranean during GI-14 and GI-13, acting as a *pull* factor (Müller et al., 2011). Potentially triggered by the Heinrich 5 event *ca*. 48 ka BP, the shift from desert-steppe environments to open woodlands in Europe and the contraction of Neanderthal populations in Europe could have paved the way for the entry of AMHs into the continent (Müller et al., 2011). The impact of Heinrich events in Africa may also have acted as a *push* factor (Carto et al. 2009). Thus, climate change may be one of the main drivers of human dispersal.

Depending on the timeframe and the region into which they dispersed AMHs developed different climatic and environmental preferences, within the wider climatic tolerances that characterize the species. To clarify these concepts, climatic tolerance acts as a limit to human adaptation while climatic preference designates optimal conditions for

the species (Davies and Gollop, 2003). Habitat suitability models reflect the probability of encountering a species and can be used to explore environmental tolerances and define preferences. Dispersals may reflect the expansion or contraction of suitable habitat (by "niche tracking") or conversely, they may reflect plasticity and broader climate preferences.

The ecological niche of AMHs, in Europe and across the globe, has been recently described as "generalist specialist" highlighting the plasticity of our species which has adapted to radically different environmental settings, becoming locally specialized in the process (Roberts and Stewart, 2018). This highlights the necessity of adopting a regional approach when studying the environmental context of AMH groups in order to disentangle local and regional scales of adaptation.

1.2 Climate variability and risk

A mark of the behavioral plasticity of human hunter-gatherers is their ability to develop new strategies to counter resource scarcity and unpredictability (Kelly, 2013). This may involve changing settlement patterns, changes in diet, technological innovations, maintaining reliable and spatially extended social networks, and changes in mobility. Resource abundance varies seasonally and annually, which is to be expected, and hunter-gatherers can anticipate these variations and alter their spatial behavior accordingly, thus ensuring their long-term survival. On the other hand, whether resource availability can be predicted or not constitutes a true ecological risk for foragers, especially in the case of key resources (Burke et al., 2017; Winterhalder et al., 1999). There is also a risk associated with mobility itself, as information about conditions at long distance locales might be deficient (Winterhalder et al., 1999). This is especially the case for dispersing populations

such as the Aurignacians who could not have extensive generational knowledge of the landscapes they encountered during dispersal.

While existing predictive models for the Aurignacian (Klein et al., 2023; Shao et al., 2021) do not discuss the impact of ecological risk, studies focused on the Last Glacial Maximum (LGM) highlight its importance in explaining site distribution, mobility, the regionalization of lithic industries and patterns of gene exchange (Burke et al., 2017; Ludwig et al., 2018; Schmidt et al., 2012; Weniger et al., 2019; Wren and Burke, 2019).

Apart from annual and seasonal climate variability and its inherent risks, the initial large-scale dispersal of AMH populations in Europe occurs during a period of important climate instability. During this timeframe several Dansgaard-Oeschger (D-O) events succeeded one another. D-O events are millennial-scale changes in atmospheric and oceanic conditions that oscillate between cold and dry conditions, correlated with Greenland Stadials (GSs), and warmer, wetter periods associated with Greenland Interstadials (GIs) (Dansgaard et al., 1982). D-O events vary in duration from a century to millennia and may be accompanied by rapid climate fluctuations that affect oceanic and atmospheric dynamics (Rasmussen et al., 2014). These fluctuations were accompanied by large-scale variations in resource production, affecting the nature and distribution of suitable human habitats (Van Andel et al., 2003). In this research we consider the impact of climate change (as structured by the millennial-scale D-O events) and climate variability (seasonal and annual) as variables of interest and discuss both scales of analysis.

1.3 The Aurignacian as proxy for AMH dispersals

In the search for the initial AMH populations to successfully disperse into Europe, we are faced with the limits of the archaeological record. The presence of hominin fossils within a layer bearing an archaeological industry is generally considered to establish the identity of its makers but technological and stylistic elements in the Chatelperronian industry and the Uluzzian industry testify to a less clear-cut association between specific biological groups and material culture (d'Errico et al., 1998; Villa et al., 2018). The multi-millennial European coexistence of AMHs and Neanderthals clearly paved the way for contacts and exchanges, and groups composed of individuals from both species as well as hybrids could also have existed and still be archaeologically invisible (Sterling, 2015). The limited quantity of human fossils available is a problem, nevertheless the Aurignacian is generally accepted to signal the appearance of *H. sapiens* (Benazzi et al., 2015; Formicola, 1989; Hublin, 2015).

This clear association allows us to use the distribution of the Aurignacian technocomplex as a proxy for modern human dispersal and mobility in Europe. In contrast, transitional industries that predate it, like the Uluzzian, the Neronian, and the Bachokirian, lack a clear association with AMHs, are mostly short-lived and lack the body of data available to discuss millennial changes on the European scale. Genetic studies show that the populations associated with the Aurignacian persisted in western European, becoming Gravettian, Solutrean and Magdalenian populations (Posth et al., 2023). We thus have data supporting the long-term success of the Aurignacian dispersal.

Some prior predictive modelling work on the Aurignacian technocomplex (Banks et al., 2013a, 2013b) was designed with the following *a priori*: the Early Aurignacian and

Proto-Aurignacian are chronologically distinct, the former emerging from the latter. This view is strongly critiqued nowadays, and the chronological and geographical coexistence of the two facies is now accepted (Barshay-Szmidt et al., 2018; Riel-Salvatore and Negrino, 2018). Based on this overlapping chronology and new technological insights highlighting a less monolithic nature to both industries (Bataille et al., 2018; Falcucci et al., 2017; Riel-Salvatore and Negrino, 2018), we made the argument elsewhere (Paquin et al., 2023) to consider both facies as part of a unified archaeological manifestation when investigating AMHs populations millennial-scale dynamics and changes in Europe.

From the archaeological evidence presented elsewhere (Paquin et al., 2023), it appears that a major AMH dispersal including the Protoaurignacian and the Early Aurignacian began around GI-12 and GS-12. The expansion phase continued through GS-10, and then slowed down with a more widespread established population all through GS-7. These observations are also coherent with the two-phase dispersal model suggested by Davies (2001, 2007) for the Aurignacian technocomplex arrival: a pioneer colonization phase characterized by low site density, low demography, and a focus on coastal locales followed by a developed phase marked by a denser site distribution, a more important demography, and settlements in a wider variety of landscapes.

In this exploration of the initial large-scale dispersal of AMHs into Europe, we ask the following research questions: a) What was the suitable habitat of AMHs during MIS 3 cold and warm phases?; b) Did climate change (D-O events) control the timing and pattern of AMH population dispersal and their expansion into Europe?; And c) Were AMHs sensitive to ecological risk, which we define as unpredictability, and does it help inform us about patterns of dispersal? We answer these questions using HS modelling, i.e., the

158 analysis of species distribution as a function of explanatory variables including climate
159 conditions (temperature, precipitation), indices of climate variability and geography, and
160 by comparing and contrasting HS models for AMHs during stadial and interstadial events.

161 Europe is an obvious choice for this study due to its well-documented
162 archaeological record and a vast body of research that seeks to explain the successful
163 dispersal of AMHs at the end of the Last Glacial. Furthermore, the scale and richness of
164 available environmental data allow for a more rigorous characterization of AMHs
165 adaptative plasticity. In this research the Aurignacian technocomplex is a proxy for the
166 large-scale dispersal of AMHs into Europe. Our analysis is based on a chronologically
167 secure archaeological database of Upper Paleolithic sites (Paquin et al., 2023). We rely on
168 this database to isolate well dated species-occurrence data for *Homo sapiens* for use in our
169 predictive modelling. This research also makes use of high-resolution paleoclimate data
170 obtained through a collaboration with the *Laboratoire des Sciences du Climat et de*
171 *l'Environement* (UMR 8212), at the *Institut Simon Laplace* (IPSL).

172 2 Materials and Methods

173 We produced a series of habitat suitability models for the Aurignacian
174 technocomplex in Europe using *Random Forest* (Breiman, 2001) a machine learning
175 algorithm. The methodology applied in the present paper is based on the protocol described
176 more fully in Burke et al. (2017). All analyses were performed using R Statistical Software
177 (v4.2.3; R Core Team 2023).

2.1 Archaeological data

The location data constituting the *presences* used in the RF models are discrete European archaeological sites containing dated, uncontested Aurignacian assemblages compiled in a previously published archaeological database (Paquin et al., 2023). Paleoenvironmental and chronological data compiled in this database are used to classify Aurignacian layers into stadial/interstadial periods. Since the environmental impact of climate conditions would not have been homogeneous across Europe, chronological data are given priority in the classification process (see Paquin et al. 2023 for more technical details). We excluded sites with chronological data that were either contested, not circumscribed enough to make a Bayesian assessment (*Amodel* index under 60, see Paquin et al., 2023), or missing. To obtain a comparable number of *presences* for the warm models, we included sites with imprecise chronological data (*Amodel* index under 60) but *in situ* paleoenvironmental data signaling warm conditions.

The result is a selection of sites divided into two groups (Table 1):1) stadial occupations (N = 37) and 2) interstadial occupations (N = 27). Some sites with multiple Aurignacian occupation layers are part of both groups, e.g., Hohle Fels, Mitoc-Malu-Galben and Les Cottés.

Warm classification

Sites	Levels	Country	Longitude	Latitude
Abri Pataud	7	France	1.01	44.94
Esquicho-Grapaou	SLC1b	France	4.32	43.93
La Ferrassie	G1	France	0.94	44.95
La Souquette	11	France	1.10	45.00
Le Flageolet I	XI	France	1.09	44.85
Le Piage	GI-F	France	1.37	44.80
Les Cottés	2	France	0.84	46.69
Šandalja II	F	Croatia	13.89	44.88
Hohle Fels	IIe, IIIa, Va & Vb	Germany	9.75	48.38
Sirgenstein	VI	Germany	9.76	48.39
Klissoura Cave 1	IIIe-g	Greece	22.81	37.69
Pes-kő	lowest layer	Hungary	20.41	48.05
Castelcivita	gic & rsa_upper	Italy	15.21	40.50

Paina	9	Italy	11.55	45.43
Riparo Bombrini	A1	Italy	7.54	43.78
Riparo Mochi	G	Italy	7.53	43.78
Lapa do Picareiro	DD	Portugal	-8.65	39.53
Mitoc-Malu-Galben	Aurignacian I inf (12b), Aurignacian I inf (11inf), Aurignacian I (11sup) & Aurignacian I (10b inf)	Romania	27.02	48.10
Mokriška jama	7	Slovenia	14.57	46.31
Potočka zijavka	7 & 5	Slovenia	14.67	46.45
El Castillo	18B1 & 18B2	Spain	-3.97	43.29
Labeko Koba	VII	Spain	-2.49	43.06
L'Arbreda	G & H	Spain	2.75	42.16
Les Mallaetes	XIVA	Spain	-0.30	39.02
Karain B	P.II	Turkey	30.57	37.08
Stranska skala IIIc	upper paleosoil	Czech Republic	16.68	49.19
Stranska skala IIIa	3	Czech Republic	16.68	49.19
Stranska skala IIa	4	Czech Republic	16.68	49.19
Stranska skala IIIb	4	Czech Republic	16.68	49.19
Bacho Kiro	6b (D)	Bulgaria	25.43	42.95
Lisen VIII	N/A	Czech Republic	16.72	49.19
Temnata Dupka	4a	Bulgaria	23.38	43.09

Cold classification

Sites	Levels	Country	Longitude	Latitude
Abri Blanchard	Bedrock_level	France	1.10	45.00
Abri Pataud	6, 11, 12, 13 & 14	France	1.01	44.94
Brignol	Limon_sablo-argileux(base)	France	0.75	44.41
Caminade-Est	G/F	France	1.25	44.87
Esquicho-Grapaou	SLC1a & BR1	France	4.32	43.93
Gatzarria	Cbf	France	-0.92	43.14
Grotte des Hyènes	2A-2C	France	-0.72	43.63
Grotte du Renne	VIII	France	3.77	47.59
Isturitz	C4d1, C4c4, C4b2 & C4b1	France	-1.21	43.35
La Crouzade	C5	France	3.09	43.13
Le Flageolet I	VIII & IX	France	1.09	44.85
Les Cottés	04lower & 04upper	France	0.84	46.69
Mladeč	D hall	Czech Republic	17.02	49.71
Trou Walou	CI-1	Belgium	5.69	50.59
Willendorf II	4	Austria	15.40	48.32
Roc de Combe	7b	France	1.35	44.77
Brillenhöhle	XIV	Germany	9.78	48.41
Friedrichsdorf-Seulberg	Loess deposit	Germany	8.65	50.24
Geißenklösterle	IIb, IId, IIIa & IIIb	Germany	9.77	48.40
Hohle Fels	IId, IIIb & IV	Germany	9.75	48.38
Höhlenstein-Stadel	Au	Germany	10.17	48.55
Vogelherd	IV	Germany	10.19	48.56
Klissoura Cave 1	IV	Greece	22.81	37.69
Fumane	D3b	Italy	10.91	45.59
Grotta del Fossellone	Layer 21	Italy	13.08	41.22
Serino	12	Italy	14.87	40.87
Lapa do Picareiro	II & GG	Portugal	-8.65	39.53
Mitoc-Malu-Galben	Aurignacian III (9b sup) & Aurignacian III sup (8b)	Romania	27.02	48.10
Divje babe I	2	Slovenia	13.91	46.11
Aitzbitarte III	Vb central	Spain	-1.89	43.26
Covalejos	B/2 & C/3	Spain	-3.93	43.39
Ekain	IXb	Spain	-2.28	43.24
El Castillo	18C	Spain	-3.97	43.29
El Cuco	III	Spain	-3.23	43.39
La Güelga	5	Spain	-5.10	43.34
La Viña	XI & XII	Spain	-5.83	43.31
Labeko Koba	IV & V	Spain	-2.49	43.06
Les Mallaetes	XII	Spain	-0.30	39.02

Table 1. Sites, occupation layers and their locational data used as presences in RF models. Coordinates are rounded to two decimals (roughly 1.1 km). The selection of sites and their coordinates were extracted from Paquin et al. (2023).

2.2 Climate simulations and downscaling

We used the Atmosphere-Ocean General Circulation Model (AOGCM) IPSL-CM5A-LR (Dufresne et al., 2013) at a ~1.9° latitude and 3.75° longitude spatial resolution to run two global climate simulations, one representing a typical MIS 3 stadial and the other a typical MIS 3 interstadial. The boundary conditions (i.e. the distribution of land, ocean and ice sheets, topography and bathymetry) are the same for both simulations and are described in Woillez et al. (2014), Le Mézo et al. (2017) and Lézine et al. (2023). These include smaller ice sheets than for the LGM (ICE_6G-C 16 kyr BP ice sheet reconstructions from Peltier et al. (2015) available at the time of running, which corresponded to the same global sea level as MIS 3). Atmospheric greenhouse concentrations are set to 205 ppm for CO_2, 500 ppb for CH_4 and 260 ppb for N_2O, as documented by ice cores, i.e. between the levels known for the pre-industrial period and for the LGM. Astronomical forcing (precession, obliquity, eccentricity) is set with values for 46 kyr BP. The MIS 3 interstadial simulation is characterized by an active Atlantic Meridional Overturning Circulation, with values ranging from 20 to 26 Sv, while the MIS 3 stadial simulation has been forced to slow down by imposing a 0.2 Sv fresh water flux at the surface of the North Atlantic Ocean, and is characterized by an AMOC ranging from 8.5 to 11 Sv.

The stadial simulation starts from the interstadial one and is run for 250 years, which is enough for the AMOC to strongly decrease. This simple set up was chosen to

obtain distinct climate states for Europe, representative of a stadial and an interstadial state, with the AMOC state being the sole driver of the differences between these states. The latest protocol for Dansgaard-Oeschger modelling studies (Malmierca-Vallet, 2023) recommends a more recent ice sheet reconstruction, but does not modify ice sheet topography or contour, or the configuration of the coastlines as they are hard to delineate due to the lack of strong chronological constraints.

From these simulations, we extracted data in the form of 50-year time series for monthly averages of sea level pressure, air temperature at 2 m above surface, relative humidity, surface wind and cloud cover. Using this data, we carried out a statistical downscaling model (GAM) (Vrac et al., 2007) to obtain precipitation and temperature at a 15 x 15 km spatial scale for MIS 3 warm and cold conditions. This statistical downscaling was only applied to a defined European study domain: longitudes between 11.57 °W and 24.74 °E and latitudes between 32.72 °N and 59.86 °N.

A GAM (Generalized Additive Model) is a statistical model used for modelling relationships between a response variable and some predictor variables, allowing for non-linear and complex associations. GAMs extend the concept of linear models by allowing each predictor to have a non-linear relationship with the response. Here, the predictors are the large-scale climate information described above and the response variable (also called "predictand") is either the temperature or the precipitation at high spatial resolution (see previous paragraph). GAM assumes that the relationship between the response variable and predictors is additive. Instead of a single linear equation, it then uses separate functions for each predictor. These functions are typically smooth and, here, we use spline functions to capture non-linear patterns. The parameters for each predictor's spline are estimated to

minimize the difference between predicted and observed values. All theoretical and technical details can be found in Vrac et al. (2007) or Latombe et al. (2018).

Using this statistical downscaling approach produces fields at the high spatial resolution needed for our analysis at a reasonable computing cost. By construction, it also corrects for the biases of the large-scale model. On the other hand, the method does not yield successive daily states of the atmosphere and land surface, as a Dynamical Regional Model would. In the present case, using the statistical method provided suitable climatic data at the adequate resolution. A comparison to similar information obtained via a Dynamical Regional Model is beyond the scope of the present study.

2.3 Candidate predictors

Variables used as candidate predictors (Table 2) of Aurignacian sites location are composed of three categories: climate variables, climate variability indices and topographical variables. All non-topographic variables were calculated separately for MIS 3 cold and warm conditions. For the climate variables, we used the outputs of the downscaled climatology to compute monthly, seasonal, and yearly averages, minima and maxima for precipitation and temperature.

For the climate variability indices, we used the downscaled outputs of the 50-year time series to calculate the standard deviation (SD) of monthly temperature averages and the coefficient of variation (CV; ratio of the standard deviation to the mean) for monthly precipitation averages at seasonal and yearly scales. Precipitation trends do not follow Gaussian distributions so the CV is a more robust choice of variability index. Other climate variability indices include the Standardized Precipitation Index (SPI) (Guttman, 1999; Hayes, 2000; McKee et al., 1993) and the Standardized Temperature Index (STI). Those

two indices display the number of months for which monthly average precipitation or temperature follow the normal trend. We calculated the SPI using the "SPEI" R package (Vicente-Serrano et al., 2010), with values standardized using a 12-month interval. We calculated the STI using the "STI" R package (Fasel, 2014).

Finally, elevation and slope, the two topographic variables included as predictors, were derived from the SRTM 90 m digital elevation model which we sampled at a 1 x 1 km scale using ArcGIS (10.8.1). The final set of candidate predictors (N = 40) is listed in Table 2.

Predictor	Type	Derivation	Description
elev	Topographic	DEM	elevation (m *asl*)
slope	Topographic	DEM	slope (reclassified) (degree)
p_avg_aut	Climatology	Climate simulation	Seasonal precipitation average, autumn (mm)
p_avg_spr	Climatology	Climate simulation	Seasonal precipitation average, spring (mm)
p_avg_sum	Climatology	Climate simulation	Seasonal precipitation average, summer (mm)
p_avg_win	Climatology	Climate simulation	Seasonal precipitation average, winter (mm)
p_avg_y	Climatology	Climate simulation	Annual precipitation average (mm)
p_max_aut	Climatology	Climate simulation	Seasonal precipitation maximum, autumn (mm)
p_max_spr	Climatology	Climate simulation	Seasonal precipitation maximum, spring (mm)
p_max_sum	Climatology	Climate simulation	Seasonal precipitation maximum, summer (mm)
p_max_win	Climatology	Climate simulation	Seasonal precipitation maximum, winter (mm)
p_min_aut	Climatology	Climate simulation	Seasonal precipitation minimum, autumn (mm)
p_min_spr	Climatology	Climate simulation	Seasonal precipitation minimum, spring (mm)
p_min_sum	Climatology	Climate simulation	Seasonal precipitation minimum, summer (mm)
p_min_win	Climatology	Climate simulation	Seasonal precipitation minimum, winter (mm)
p_var_aut	Climate variability	Climate simulation	Seasonal precipitation, coeff. var., autumn
p_var_spr	Climate variability	Climate simulation	Seasonal precipitation, coeff. var., spring
p_var_sum	Climate variability	Climate simulation	Seasonal precipitation, coeff. var., summer
p_var_win	Climate variability	Climate simulation	Seasonal precipitation, coeff. var., winter
p_var_y	Climate variability	Climate simulation	Seasonal precipitation, coeff. var., yearly
spi_norm	Climate variability	Climate simulation	N months within normal (predicted) precipitation range
sti_norm	Climate variability	Climate simulation	N months within normal (predicted) temperature range
t_avg_aut	Climatology	Climate simulation	Seasonal temperature average, autumn (°C/10)
t_avg_spr	Climatology	Climate simulation	Seasonal temperature average, spring (°C/10)
t_avg_sum	Climatology	Climate simulation	Seasonal temperature average, summer (°C/10)
t_avg_win	Climatology	Climate simulation	Seasonal temperature average, winter (°C/10)
t_avg_y	Climatology	Climate simulation	Yearly temperature average (°C/10)
t_max_aut	Climatology	Climate simulation	Seasonal temperature maximum, autumn (°C/10)
t_max_spr	Climatology	Climate simulation	Seasonal temperature maximum, spring (°C/10)
t_max_sum	Climatology	Climate simulation	Seasonal temperature maximum, summer (°C/10)
t_max_win	Climatology	Climate simulation	Seasonal temperature maximum, winter (°C/10)
t_min_aut	Climatology	Climate simulation	Seasonal temperature minimum, winter (°C/10)
t_min_spr	Climatology	Climate simulation	Seasonal temperature minimum, spring (°C/10)
t_min_sum	Climatology	Climate simulation	Seasonal temperature minimum, summer (°C/10)
t_min_win	Climatology	Climate simulation	Seasonal temperature minimum, winter (°C/10)
t_sd_aut	Climate variability	Climate simulation	Standard deviation, seasonal temperature, autumn
t_sd_spr	Climate variability	Climate simulation	Standard deviation, seasonal temperature, spring
t_sd_sum	Climate variability	Climate simulation	Standard deviation, seasonal temperature, summer
t_sd_win	Climate variability	Climate simulation	Standard deviation, seasonal temperature, winter
t_sd_y	Climate variability	Climate simulation	Standard deviation, temperature, yearly

Table 2. List of predictors included in the modelling process.

2.4 Data preparation

In addition to the selection of archaeological sites to act as presences (see above) the modelling process requires a library of pseudo-absences from which to draw upon. To this end, the climate data issued from the statistical downscaling were interpolated using the "natural neighbor interpolation" tool and resampled to create 1 km resolution rasters for each of the 40 variables from both the warm and cold paleoclimatic conditions. Next, we produced two point feature classes with 1 x 1 km spacing, one for stadial conditions and one for interstadial conditions, and extracted predictor values from the rasters to the points. The point feature classes were then clipped using masks of the current coastline configuration and the extent of the LGM ice sheets (Ehlers et al., 2011). Additionally, 10 km radius buffers were created around archaeological sites included in the study. This serves to exclude the more immediate foraging territory of Aurignacian occupations from the *pseudo-absence* datasets.

Presences were generated by loading the georeferenced archaeological sites into point feature classes and extracting the predictor values from the rasters, as described above. To minimize the chances of overfitting, we created 1 km radius buffers around each site and checked for overlaps. Sites with overlapping buffers were deemed too close to one another and were counted as a single *presence*.

Finally, for both the warm and cold datasets, the *presence* and the *pseudo-absence* point feature classes were merged into two discrete feature classes and the attribute tables exported into csv files for use in the next step.

2.5 Random Forest parameterization and model fitting

Random forest (RF) is a nonparametric algorithm for regression and variable selection that uses decision trees (Breiman, 2001). We used RF to build habitat suitability models for the Aurignacian under stadial and interstadial conditions. We chose this algorithm for its ability to handle non-linear relationships, large numbers of predictors and small datasets of *presence* observations (Genuer et al., 2010; Grömping, 2009).

First, we identified highly correlated predictor variables within the datasets using the *findCorrelation* function in the "caret" R package with a cut-off value of 0.8. Once correlated pairs were identified, the variable with the higher mean correlation with all other variables was removed. We supervised the process, prioritizing seasonal variables over yearly averages, such as spring temperatures (Kim et al., 2014) which has a demonstrated impact on vegetation productivity. This process resulted in the retention of 25 uncorrelated variables for the warm dataset and 23 for the cold dataset (see SI.3).

The filtered lists of variables were then used as candidate predictors in an iterative variable selection process using RF (Fig. 1). The most robust performances for RF are obtained by averaging multiple runs of a model combined with a relatively low number of *pseudo-absences* (Barbet-Massin et al., 2012). Using the *RF* function from the "caret" R package, we ran each model for 100 runs with 10-fold cross-validation and equal numbers of randomly selected *pseudo-absences* and *presences* (N = 37 for the cold models and N = 27 for the warm models) (Barbet-Massin et al., 2012). We used default values for the *n-tree* (N = 500; the number of trees to grow for each model) and an *m-try* value of $\sqrt{p}$ (p = number of predictors; *m-try* designates the number of randomly selected predictors interrogated at each split or node) (Díaz-Uriarte and Alvarez de Andrés, 2006). Model

accuracy was calculated using the area under the Receiver Operating Curve (ROC). Accuracy, the Out-of-the-Bag (OOB) error rate and the Variable Importance indices (VI) were calculated for each run and averaged to assess model performance for each iteration (the script is included in supplementary information).

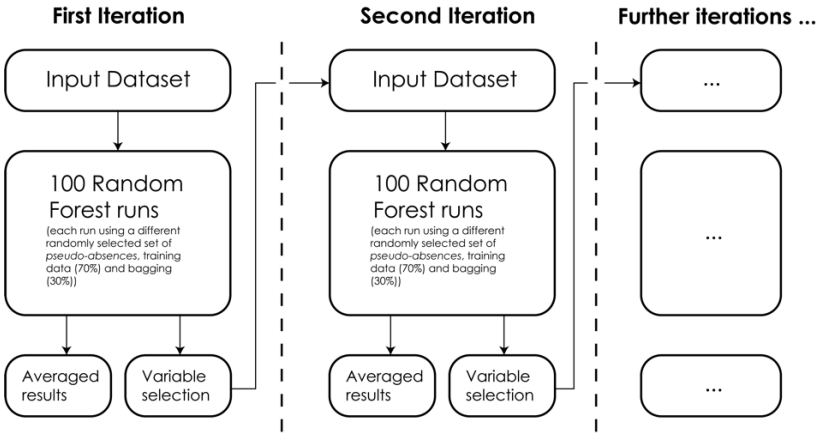

Figure 1. Random Forest iterative variable selection process.

The iterative variable selection process used the VI metric to identify the least important predictors (the bottom 20%) which were removed before the next iteration of 100 runs, and so on. OOB and model accuracy were then used conjointly to identify which run produced the model with the most robust results while being the most parsimonious. The HS scores from the selected RF models were then mapped.

The list of predictors from the best models were then tested using a Generalized Linear Model (GLM) to identify which predictors have linear relationships with the dependent variable (see SI.2 for results). This test was done using the *GLM* function in the "caret" R package with 10 times as many *pseudo-absences* as *presences* as suggested by Wisz & Guisan (2009). Once again, we ran the model 100 times before averaging the results.

3 Results

For the warm and cold datasets, the final models are illustrated in Fig. 2 & Fig. 3 and the RF predictions produced at each step of the variable selection process are illustrated in the supplementary information (SI.4). The variable importance index (VI), which measures the relative importance of the predictors, is presented in Table 3 and Table 4 for each iteration. Model performance (OOB and accuracy) is presented in Table 5 and 6 and illustrated in Fig. 4.

For the warm dataset, associated with GI conditions, the best model performance was obtained with the model *6var*, containing 6 predictors. For the cold dataset, associated with GS conditions, the best model performance was obtained with the model *6var*, also containing 6 predictors. Both these models are also the most parsimonious choices since they had the lowest OOB of their groups and no simpler model produced an OOB situated within 1 standard error of their respective scores (Fig. 4). As for the accuracy, both are within 1 standard error of the highest accuracy of their respective series. Because of this, they were chosen as the final *habitat suitability* models. Results for the additional GLM tests of these 2 winning models are included in the supplementary information (see SI.2).

For the warm HS model, the predictors included (Table 3; Fig. 5 & 7), in order of importance (VI), are: *slope*, *p_var_spr* (coefficient of variability for spring precipitation), *t_avg_aut* (averaged monthly temperatures for Autumn), *p_max_spr* (maximum monthly average precipitations for spring), *p_var_win* (coefficient of variability for winter precipitation) and *elevation*.

For the cold HS model, the predictors included (Table 4; Fig. 6 & 8), in order of importance (VI), are: *p_min_aut* (minimum monthly average precipitations for autumn), *slope*, *t_sd_aut* (standard deviation in average monthly temperatures in autumn), *p_min_sum* (minimum monthly average precipitations for summer), *t_sd_sum* (standard deviation in average monthly temperatures in summer) and *elevation*.

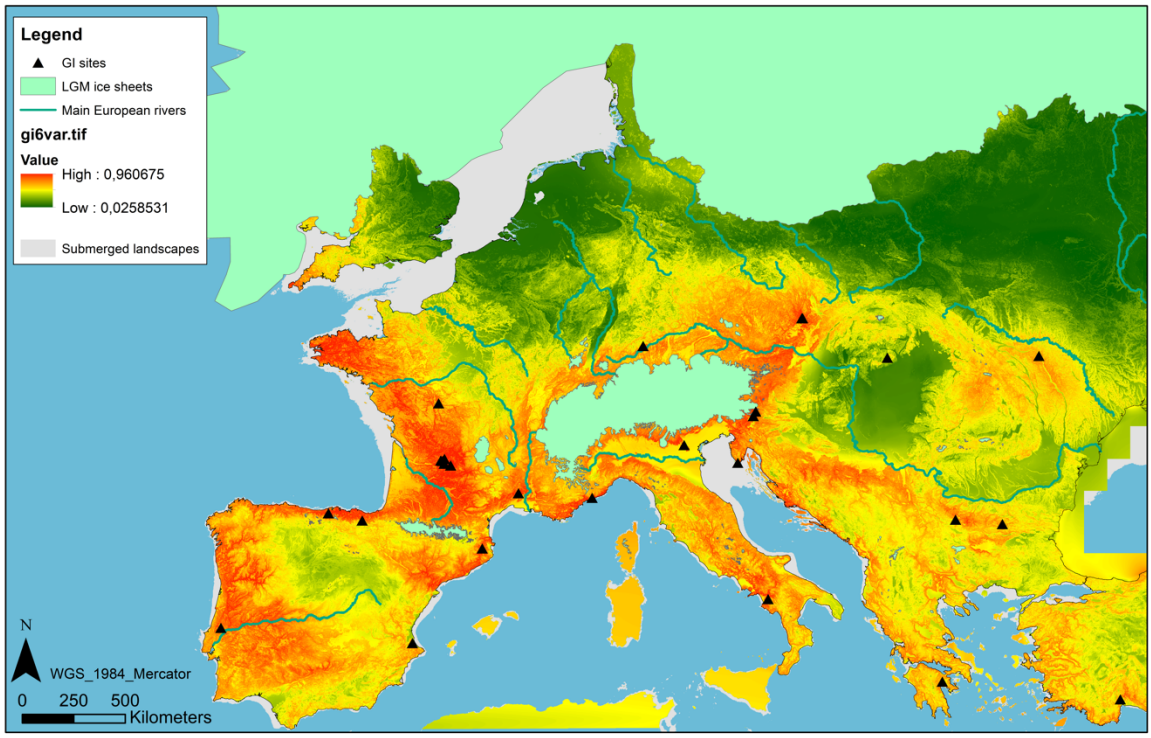

Figure 2. Final warm model 6var. The sites used as presences are displayed over the Habitat Suitability (HS) index. The LGM ice sheets are downloaded from Ehlers et al., 2011 and simplified to remove holes in the Alps. The submerged landscapes areas were produced by Albouy et al., 2023.

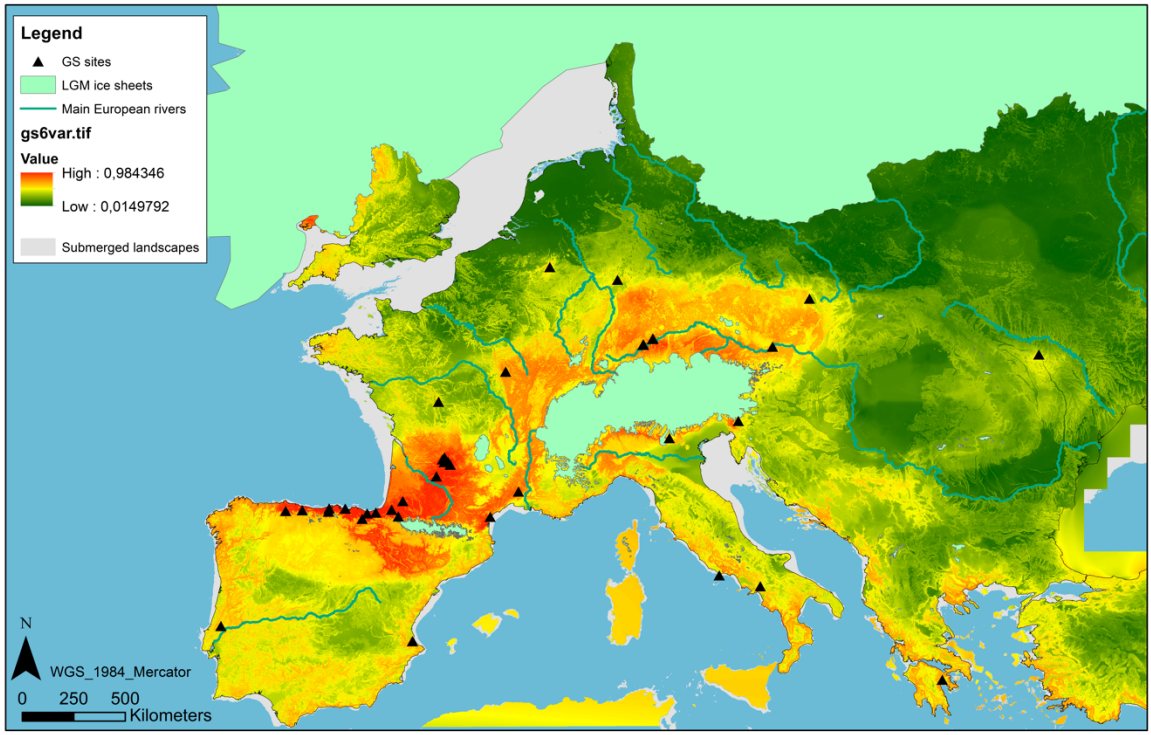

Figure 3. Final cold model 6var. The sites used as presences are displayed over the Habitat Suitability (HS) index. The LGM ice sheets are downloaded from Ehlers et al. 2011. The paleoshorelines were produced by Albouy et al., 2023.

25var	VI	20var	VI	16var	VI	13var	VI	10var	VI	8var	VI	6var	VI	5var	VI	4var	VI	3var	VI
slope	78.68	slope	82.67	Slope	85.92	slope	83.65	slope	81.71	slope	78.42	slope	79.83	slope	82.85	slope	76.32	slope	69.14
p_var_spr	42.08	p_var_spr	48.05	p_var_spr	36.88	p_var_spr	38.87	p_var_spr	41.46	p_var_spr	46.78	p_var_spr	58.55	p_var_spr	45,06	p_var_spr	48,48	p_var_spr	49,81
t_sd_aut	31,06	t_avg_aut	37,21	t_avg_aut	33,35	t_avg_aut	35,29	t_avg_aut	31,24	t_avg_aut	41,23	t_avg_aut	39,39	t_avg_aut	32,95	t_avg_aut	25,90	t_avg_aut	27,48
p_var_sum	30,40	t_sd_aut	34,27	p_max_spr	32,10	p_var_win	27,49	p_max_spr	30,37	p_var_win	28,89	p_max_spr	25,74	p_var_win	29,64	p_var_win	21,44		
p_max_spr	30,36	p_max_spr	33,11	p_var_win	31,36	elev	27,41	p_var_sum	30,13	elev	27,67	p_var_win	22,45	p_max_spr	22,57				
t_avg_aut	29,33	p_var_sum	30,79	Elev	27,48	t_sd_aut	26,93	elev	28,25	p_max_spr	26,75	elev	20,98						
elev	29,11	p_var_win	28,12	p_var_sum	26,63	p_var_sum	26,18	p_var_win	26,37	p_var_sum	23,93								
p_max_aut	27,49	p_var_y	27,79	p_var_y	26,53	p_max_spr	24,87	p_var_y	26,20	p_var_y	23,25								
p_var_win	27,47	p_max_sum	26,93	t_sd_aut	26,15	p_max_sum	24,10	t_sd_aut	25,75										
p_var_y	24,31	p_min_aut	26,64	p_max_sum	23,63	p_var_y	23,61	p_max_sum	24,05										
p_min_aut	23,80	p_max_aut	25,47	p_min_aut	23,51	p_max_aut	22,98												
p_max_sum	22,41	elev	25,14	p_max_aut	22,53	p_min_aut	21,45												
p_min_sum	19,83	t_sd_win	22,24	t_sd_sum	18,55	t_sd_sum	16,61												
p_max_win	19,42	t_sd_sum	21,24	p_max_win	16,30														
sti_norm	18,63	p_max_win	18,42	t_sd_win	14,14														
t_sd_win	18,28	p_var_aut	17,61	p_var_aut	12,53														
t_sd_sum	18,06	sti_norm	17,32																
spi_norm	14,90	p_min_sum	17,14																
p_min_win	14,34	p_min_win	17,13																
p_var_aut	13,73	spi_norm	11.91																
p_avg_y	13.31																		
t_min_sum	12.42																		
t_max_spr	11.76																		
p_min_spr	10.97																		
p_avg_sum	10.11																		

Table 3. Variable Importance (VI) of the variables tested for each of the warm conditions models.

23var	VI	19var	VI	16var	VI	13var	VI	10var	VI	8var	VI	6var	VI	5var	VI	4var	VI	3var	VI
p_min_aut	72,35	p_min_aut	73,59	p_min_aut	70,70	p_min_aut	70,45	p_min_aut	75,65	p_min_aut	76,37	p_min_aut	73.19	p_min_aut	74.38	p_min_aut	74.63	p_min_aut	78.70
slope	53.79	p_min_sum	54.85	Slope	54.61	p_min_sum	49.02	p_min_sum	50.64	Slope	53.90	slope	51.45	slope	48.46	slope	39.38	slope	39.74
p_min_sum	53.24	slope	45.03	p_min_sum	50.00	slope	47.45	slope	50.11	p_min_sum	48.26	t_sd_aut	44.04	t_sd_sum	33.29	t_sd_sum	38.07	t_sd_sum	26.69
t_sd_aut	49.74	t_sd_aut	40.59	t_sd_aut	42,22	elev	36,45	t_sd_aut	36,21	t_sd_aut	36,08	p_min_sum	40,83	p_min_sum	30,70	p_min_sum	31,77		
t_sd_sum	40,15	elev	38,39	Elev	37,81	t_sd_aut	35,60	elev	35,23	Elev	34,89	t_sd_sum	31,75	t_sd_aut	27,04				
elev	38,01	t_sd_sum	33,33	sti_norm	33,12	sti_norm	29,32	t_sd_sum	31,30	t_sd_sum	25,44	elev	25,18						
sti_norm	37,58	sti_norm	33,12	t_sd_sum	29,24	t_sd_sum	27,44	p_min_spr	28,56	p_min_spr	21,68								
p_min_spr	34,13	p_var_sum	30,49	p_min_spr	28,33	p_var_sum	26,64	sti_norm	26,45	sti_norm	20,82								
p_max_win	32,00	p_min_spr	29,95	p_var_sum	26,27	p_max_win	23,60	p_var_sum	24,21										
p_var_sum	29,59	p_max_win	29,58	p_max_win	23,46	p_min_spr	23,16	p_max_win	23,56										
p_var_spr	28,28	p_var_aut	27,88	p_var_aut	22,32	p_var_aut	22,56												
p_var_aut	28,22	p_var_spr	24,99	spi_norm	21,86	p_var_spr	21,72												
p_var_win	26,69	spi_norm	19,92	p_var_spr	21,60	spi_norm	17,36												
spi_norm	26,13	p_max_spr	19,10	p_var_win	21,39														
p_max_spr	22,08	t_avg_aut	18,58	p_max_spr	21,07														
t_avg_aut	20,71	p_var_win	17,18	t_avg_aut	18,45														
p_avg_y	20,06	p_avg_y	16,08																
t_min_sum	17,14	p_max_aut	13.01																
p_max_aut	15.21	t_min_sum	10.98																
p_max_sum	14.63																		
t_sd_win	12.40																		
p_min_win	11.34																		
t_max_spr	4.38																		

Table 4. Variable Importance (VI) of the variables tested for each of the cold conditions models.

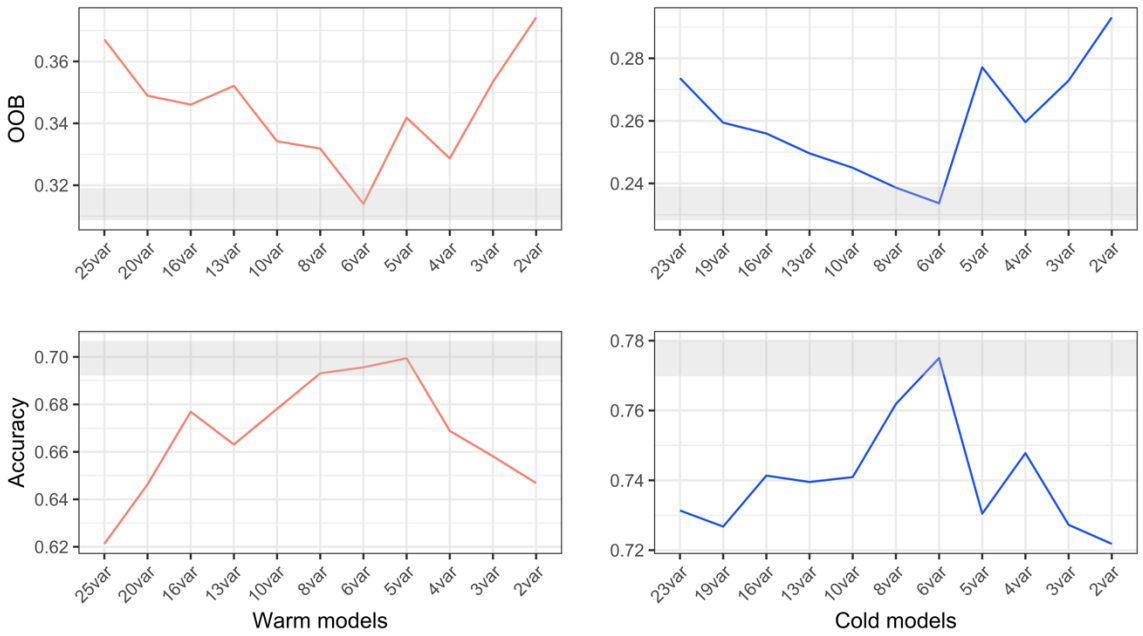

Figure 4. OOB and accuracy graphs for warm and cold models at each step. The grayed areas represent 1 standard error (SE) over and under the lowest OOB score or the highest accuracy score for each series.

Models	OOB	accuracy	N predictors
25var	0,367	0,621	25
20var	0,349	0,646	20
16var	0,346	0,677	16
13var	0,352	0,663	13
10var	0,334	0,678	10
8var	0,332	0,693	8
6var	0,314	0,696	6
5var	0,342	0,699	5
4var	0,329	0,669	4
3var	0,353	0,658	3
2var	0,374	0,647	2

Table 5. Performances of the warm models at each step.

Models	OOB	accuracy	N predictors
23var	0,274	0,731	23
19var	0,259	0,727	19
16var	0,256	0,741	16
13var	0,250	0,740	13
10var	0,245	0,741	10
8var	0,239	0,762	8
6var	0,234	0,775	6
5var	0,277	0,730	5
4var	0,260	0,748	4
3var	0,273	0,727	3
2var	0,293	0,722	2

Table 6. Performances of the cold models at each step.

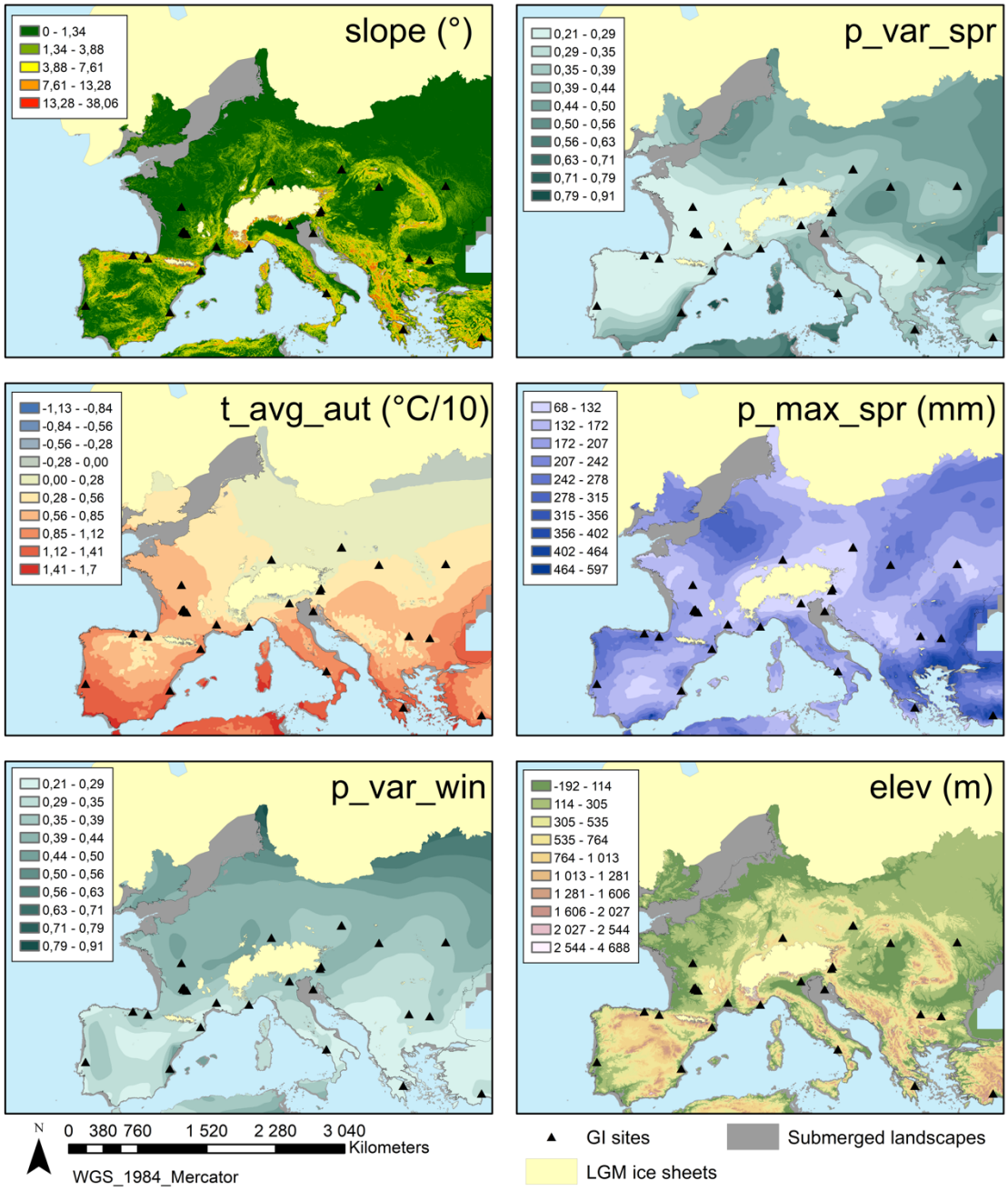

379

380 **Figure 5**. Predictors included in the warm model 6var mapped according to GI conditions.

381 The unit for p_var_spr & p_var_win is the coefficient of variation.

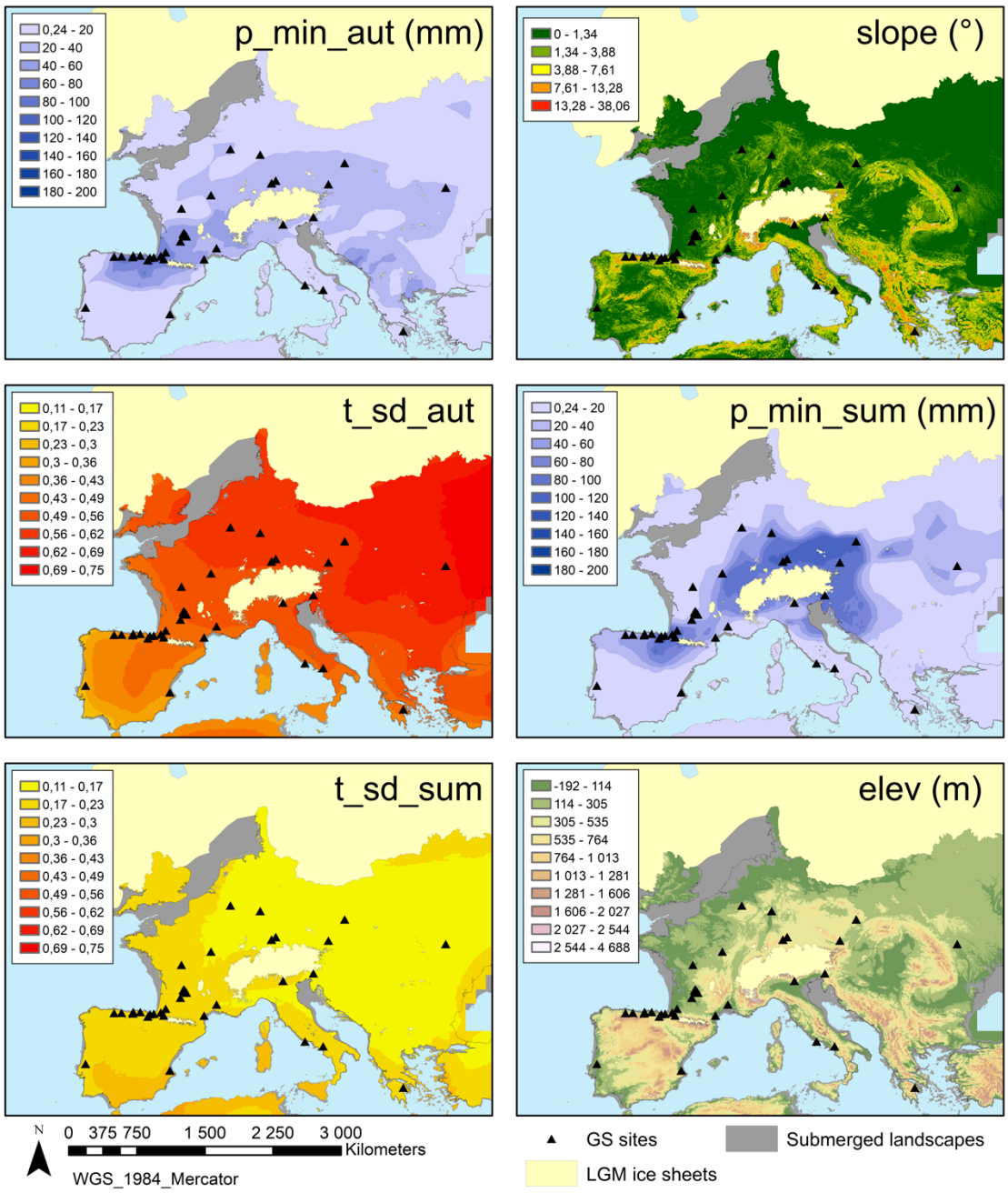

382

383 **Figure 6**. Predictors included in the cold model 6var mapped according to GS conditions.

384 The unit for t_sd_aut & t_sd_sum is the standard deviation.

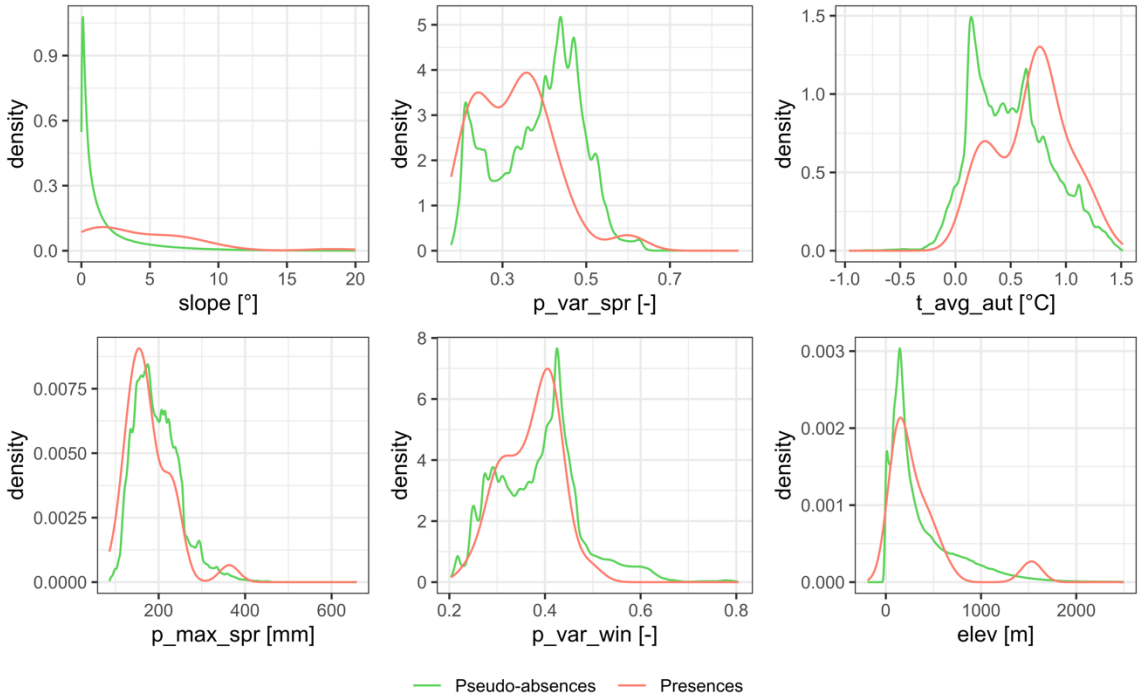

385

386 **Figure 7.** Density plots (presences and pseudo-absences) for the predictors included in

387 the warm habitat suitability model 6var. Variables are presented in order of importance

388 (VI) from left to right starting with the first row.

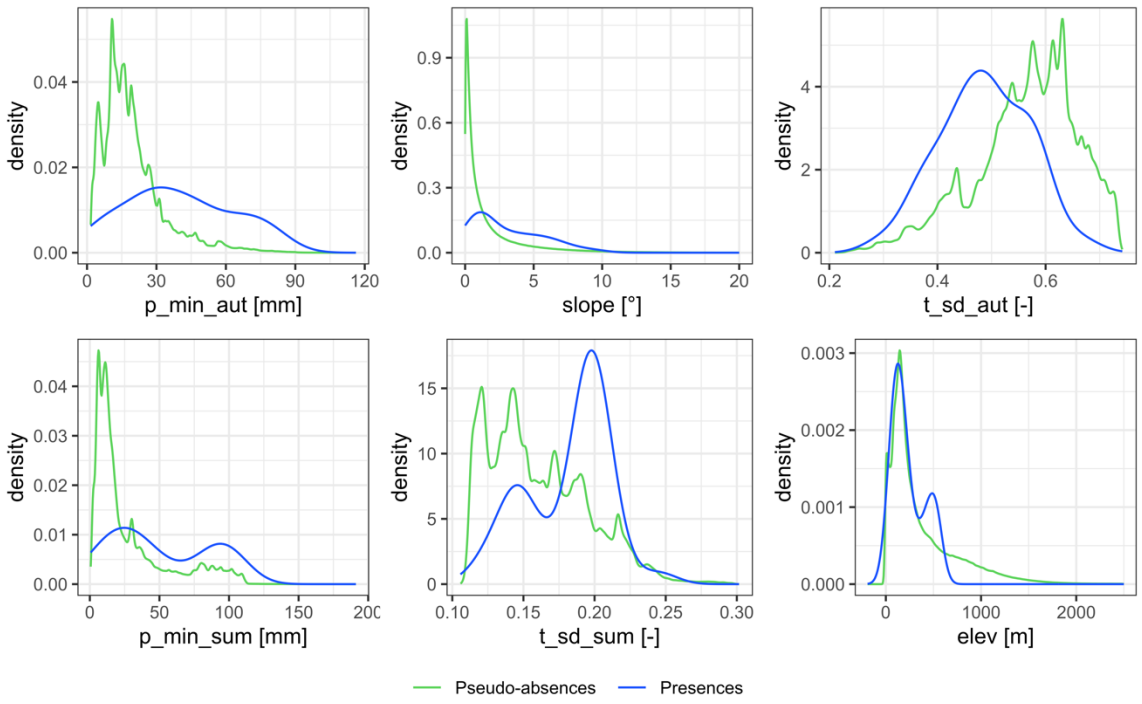

389

390 **Figure 8.** Density plots (presences and pseudo-absences) for the predictors included in the
391 cold habitat suitability model 6var. Variables are presented in order of importance (VI)
392 from left to right starting with the first row.

393 # 4 Discussion

394 ## 4.1 Habitat Suitability predictive models

395 HS is a proxy for the carrying capacity of the landscape, and the HS index indicates
396 the probability of encountering humans on the landscape. In other words, it is to be
397 expected that the number of archaeological sites will be reduced or absent from areas with
398 low HS values. The final predictive models for GIs and GSs display distinct spatial
399 structures of suitable habitat (Fig. 2 & 3). The warm model produces a geographically
400 larger area of suitable habitat in Europe while the cold model indicates a considerably more
401 restricted one. Figure 9 illustrates this expansion of suitable habitat during GIs; the

percentage of the European domain associated with higher HS scores for the warm model is greater than the cold model. The cold model shows that higher values of HS are concentrated in South-West France and the Northern Iberian peninsula, but also in the Danube watershed West of the Carpathian Basin (Fig. 3). High values of HS during GIs expand from these landscapes towards other regions, such as Brittany, the Iberian Peninsula, Italy and the Balkans (Fig. 2).

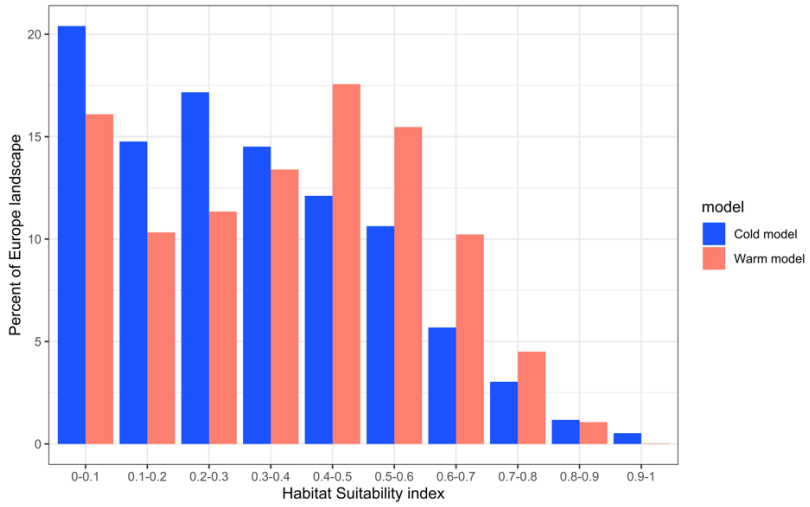

Figure 9. Percentage bar plot comparing the habitat suitability outputs produced by the warm and the cold models and their spatial extent.

Despite a relatively smaller area of suitable habitat, there are more sites during GSs. This doesn't necessarily mean that site densities are greater, however, because the stadial events represent a longer interval of time than the interstadials. In a prior study, we took the third dimension (time) into account and calculated a chronological density index for Aurignacian occupations during stadials and interstadials (Paquin et al., 2023). This index controls for the duration of these climatic phases. We highlighted that GSs generally have a higher chronological density of Aurignacian occupations than GIs. We argued that an

418 intensified pattern of residential mobility during GSs could explain this phenomenon,
419 rather than an increase in population density. The contraction of suitable habitat during
420 GSs, observed above, supports this idea if we consider that populations contracted their
421 ranges.

422 For the warm model, the lowest HS scores associated with Aurignacian sites within
423 our dataset all occur in Eastern Europe: *Mitoc-Malu-Galben* (0.63), *Pes-kő* (0.63) and
424 *Bacho Kiro* (0.65) and *klissoura* (0.67) (Fig. 2). The picture is more geographically diverse
425 for the cold model, highlighting relatively worse climatic conditions across the continent
426 during stadials. The archaeological sample could be playing a causal role here: the
427 Aurignacian technocomplex is documented in numerous sites in Eastern Europe,
428 particularly in the Carpathian Basin (Floss et al., 2016; Hauck et al., 2018) but very few of
429 these sites, other than *Pes-kő* and *Mitoc-Malu-Galben,* offer chronological and/or
430 paleoenvironmental data precise or robust enough to classify occupations as pertaining to
431 cold or warm conditions. Most of the eastern European sites are thus not included in our
432 database. These scores could also reflect relatively poorer conditions in Eastern Europe
433 during warm phases. While HS is visibly worse in Eastern Europe than it is in the West
434 during stadials (Fig. 3), the warm model maps show generally good HS values in the east,
435 but still lower than Western Europe (Fig. 2).

436 The Aurignacian technocomplex is relatively well represented in the archaeological
437 record of northwestern France, e.g. multiple sites exist in Brittany, such as *Beg-ar-C'hastel*
438 and *Îlot des Agneaux* (Hinguant and Monnier, 2013). Even further north, on the British
439 Isles, the Aurignacian is documented at sites such as *Kent's Cavern*, although occupation
440 of the territory is believed to have been punctual and sporadic (Dinnis, 2012). The model

441 indicates that Britanny was a highly suitable landscape for Aurignacian people during GIs.
442 This is interesting because, due to the lack of robust chronological data, we did not use
443 Aurignacian sites from this region to train the model. Most of the Breton sites are coastal
444 and fall within relatively good HS indices according to the warm model. Lacking
445 archaeological knowledge pertaining to submerged landscapes under the Channel
446 considerably limits our understanding of Aurignacian mobility in this region. It is plausible
447 that conditions were suitable during GIs on both sides of the Channel.

448 The warm model indicates that the HS index is quite high in most of the Iberian
449 Peninsula even though few sites in our database, apart from those in the Northern coastal
450 region, attest to an Aurignacian presence. The two sites in our dataset that are further south
451 of the Peninsula are *Lapa do Picareiro* and *Les Mallaetes*, the former of which could have
452 been occupied as early as GI-11 with a terminus post quem of 41.9 – 41.1 cal ka BP (Haws
453 et al., 2020). *Les Mallaetes* is occupied much later by Aurignacian groups around GI-8 and
454 GS-7 (Paquin et al., 2023; Villaverde et al., 2021). Our models indicate that Iberian
455 landscapes were generally suitable for AMH settlement during the warm phases of MIS 3.
456 These results could be consistent with the Ebro River hypothesis, which predicts that the
457 presence of Neanderthal populations South of the Ebro slowed the dispersal of AMHs into
458 central and southern Iberia (Zilhão, 2000). Evidence for an Early Aurignacian presence at
459 *Lapa do Picareiro* recently cast doubt on the Ebro river hypothesis (Haws et al., 2020),
460 however, but the debate is ongoing (Zilhão, 2021).

461 ## 4.2 Predictors

462 RF classification allows for the identification of strong predictors among a large
463 series of variables for explaining site location. Nevertheless, as it considers interactions

between variables, a drawback of the method is the difficulty interpreting the impact of individual predictors. We applied a mixed approach to address this issue, using the variables included in the best RF models to produce GLM models (see SI.2). This made it possible to identify predictors that have a linear relationship with the dependent variable: site location. Topographic variables for elevation and slope display a linear relationship with site location in both models. Otherwise, the only other variable with a linear relationship is the minimum precipitation rate for Summer in the cold model. All other predictors included present non-linear relationships with the dependent variable and are only interpretable in conjunction with other variables.

Therefore, we use density graphs produced during the RF runs to interpret the relationship of the predictors with HS values. Some trends are visible in the density graphs (Fig. 7 & 8). Slope values for both GI and GS suggest a preference for slightly sloping, rather than flat ground, which would potentially be floodplains. Even if slope explains site location in a linear fashion (see SI.2), there is an apparent upper threshold at 10 degrees. Sites tend to be located under 700 m elevation, although there is a peak around 1500 m during GIs that could indicate movement to highland regions during warm phases.

Cells with lower variability in precipitation rates during spring and winter are disproportionately represented during GIs, although this effect is less pronounced in winter (Fig. 7). This implies that predictable patterns of precipitation influenced human spatial decisions, particularly in spring. Additionally for the GIs, higher than average temperatures in autumn are over-represented, as are slightly lower maximum spring precipitation rates.

There's a notable trend towards a selection for lower variance in autumn temperatures during stadials (Fig.8). This makes sense in terms of the human perception of

ecological risk and risk management; locales with predictable autumn temperatures could ensure access to and availability of needed resources before the winter months. Variance in temperature gravitates towards higher values during summer. It could be that variance in summer temperature is linked to other variables included in the model. This predictor also has a relatively high correlation coefficient with autumn temperature variance: *t_sd_aut* and *t_sd_sum* are inversely correlated by a coefficient of -0.74, just under the 0.8 cut-off used in the modelling process. Minimum precipitation rates trend towards higher values for both autumn and summer, extending the growing season, but especially in autumn when, as noted above, lower temperature variance is selected for.

4.3 Addressing climate risk and dispersal routes

One of the main advantages of the paleoclimatic reconstructions on which the models are built is the ability to calculate inter- and intra-annual variability in temperature and precipitation. This information allows us to test human sensitivity to climate variability at different scales and opens the door to a discussion on ecological risk. Both final HS models include predictors pertaining to climate variability which we consider an element of ecological risk (and see Burke et al., 2017) indicating that the predictable distribution of resources was clearly a factor in habitat suitability.

The lowest HS scores associated with Aurignacian sites included in the models highlight differences between GIs and GSs. The lowest site for the GIs is associated with an HS index of 0.63 while the 4 lowest scores associated with GS sites are all lower than this: *Mitoc-Malu-Galben* (0.52), *Serino* (0.56), *Les Cottés* (0.59) and *Friedrichsdorf-Seulberg* (0.6). The threshold at which cells with low HS values are really occupied is thus considerably lower during GSs. Two of these sites include multiple Aurignacian levels;

Mitoc-Malu-Galben is occupied during different interstadials and stadials from GI-8 to GS-5.2 while Les Cottés comprises three Aurignacian layers associated with GI-9 and GS-9. The lower HS threshold during stadials could mean that humans would have continued to occupy known sites even if conditions were not ideal.

The lower HS threshold during GSs, added to the observation that the proportion of habitable landmass shrank (Fig. 9), could indicate that human populations had to adjust to sub-optimal conditions, highlighting the ecological stresses to which they had to adapt. The cold model can thus illustrate the climate tolerance of early European AMHs. With a wider choice of regions in which humans could settle, as underlined by the higher proportion of the habitable landmass (Fig. 9) and a higher HS threshold, the warm model indicates the climate preference of Aurignacian groups. If populations were trying to maintain themselves during stadials without densely populating highly suitable zones, they would have inevitably ended up in less suitable areas, hence the lower GS threshold.

It is also relevant to note that conditions were not homogeneous across Europe during specific climatic phases. Some sites with occupations classified as stadial due to chronological data, like Covalejos in Northern Spain or the Grotte du Renne, in France, display paleoenvironmental data indicating somewhat warm conditions (see Paquin et al., 2023 for additional examples). For instance, Covalejos level C/3 faunal assemblage exhibits a mosaic of deer, horse and bos (Yravedra et al., 2016; Jones et al., 2019) while palynology indicates both steppe and temperate species (Ruiz-Zapata & Gil, 2005). Both cold and warm conditions are signaled by this kind of pattern, which could indicate some resource or niche tracking by Aurignacian populations during GS periods as a form of risk reduction strategy.

As mentioned above, our results show that AMHs were affected by climate variability and climate change during the MIS 3 and adapted by altering their range. Fitness related innovations also explain AMH adaptive capacity to climate change. Specialized cold climate clothing, for example, was potentially made and worn by Aurignacian groups (Collard et al., 2016). A broadening of the AMH diet by the intensification of small prey exploitation during the Aurignacian (Llovera et al., 2016) is also a good example of such adaptations. Technical and behavioral adaptations, such as those mentioned here, probably participated in making AMHs the sole hominin species to survive the unstable climate of MIS 3 and the onset of the LGM in the long run. The question of Neanderthal's disappearance is not the focus of the present study and depends on many factors, including the possibility of competitive exclusion (Timmermann, 2020). Decreasing available biomass (Vidal-Cordasco et al., 2022) or a repeated fragmentation and reduction of the habitable landmass before the arrival of AMH populations (Melchionna et al.,2018; Klein et al., 2023) are also aspects to take into consideration.

In our previous paper we presented data suggesting an initial dispersal phase (approximately between GI-12 and GI-10) marked by the quick expansion of Aurignacian groups, indicated by a steadily increasing chronological density of archaeological occupations, followed by an established population phase starting around GS-10 with a more widespread occupation of Europe (Paquin et al., 2023). During the initial dispersal phase, Aurignacian sites are mainly located in coastal environments, principally the Mediterranean coast, with some occupations in the Danube valley, in Germany and Austria. The question remains as to whether there was a single entry point, or multiple entry points

555 for initial Aurignacian dispersal into Europe and the two main migration routes proposed
556 are along the Mediterranean coastline and the Danube valley (Mellars 2011).

557 The models produced in this study show contrasting patterns of habitat suitability
558 on the Mediterranean coast between cold and warm cycles (Fig. 2 & 3). During GSs,
559 suitable habitats along the Mediterranean coast exist as discontinuous patches. Otherwise,
560 coastal regions are mainly composed of medium and low HS values. During GIs, the HS
561 values along the coast are higher and form a continuous corridor of suitable habitat. For
562 the Danube valley route, both models show favorable habitat in the western portion of the
563 route but from the Carpathian Basin eastward, HS values are low (especially for GS) and
564 only a few chronologically controlled Aurignacian sites are known (Fig. 2 & 3). As
565 mentioned earlier, however, our database is incomplete in Eastern Europe and the HS
566 models suggest that both routes would have been plausible entry points during GIs, with
567 the Mediterranean coast being relatively more favorable. Submerged landscapes which are
568 invisible in our data could very well have extended this putative dispersal route (Fig. 2).

569 Still, the Danube valley, mainly for the region north of the Alps, could have been a
570 corridor of mobility in continental Europe during GSs, considering the relatively high HS
571 values and the persistent presence of Upper Paleolithic occupations in the region. Our
572 models could support certain aspects of the *Kulturpumpe* hypothesis, therefore (Conard
573 and Bolus, 2003). We are not suggesting that the Early Aurignacian emerges from this
574 region, but that, once settled, it could have acted as a cultural core area during most of
575 MIS 3. The Rhone Valley, another important biogeographic corridor linking the
576 Mediterranean coastline to Central Europe, is equally suitable during warm or cold
577 conditions (Fig. 2 & 3).

4.4 Comparison with other published models

Other studies have integrated archaeological site location data and paleoclimate reconstructions to evaluate the Aurignacian habitat in Europe (e.g., Banks et al., 2013a, b; Shao et al., 2021; Timmermann, 2020; Klein et al., 2023). Our results agree with these (and other) studies which conclude that climate change had an impact on human populations and spatial behavior during MIS 3, since our results clearly indicate that suitable habitat contracted considerably during GSs.

Continental-scale models (Shao et al., 2021), as well as modelling focused on the Iberian Peninsula (Klein et al., 2023) also incorporate climate variability predictors in computing the human existence potential (HEP) for the Aurignacian, an index which is conceptually equivalent to the habitat suitability score we use here. Nevertheless, they only include as predictors the annual means for temperature and precipitation variability, which limits the scope at which they can discuss the concept of ecological risk. The inclusion of seasonal variability predictors in our study allows interpretable results regarding this research theme. Klein et al.'s (2023) model highlights the importance of the Franco-Cantabrian region across GI/GS cycles, which is consistent with our results. But Shao et al.'s (2021) models show a GS contraction of the HEP area towards the Mediterranean region, leaving two of the core areas of Aurignacian occupations, Franco-Cantabria and the Danube valley North of the Alps, with low HEP values. Our cold conditions model shows contrasting results, with a contraction of the habitat centered around these archaeologically important regions during stadials.

Another recent study models Neanderthals and AMHs dispersals using climate forcing to evaluate the impact of interbreeding, competitive exclusion and D-O oscillations

on the disappearance of the former species (Timmermann, 2020). This research concludes that Neanderthal extinction cannot be understood simply by climate change, and that a more realistic scenario should include arriving AMH populations with higher degrees of plasticity, mobility and fecundity. Our study supports this idea by demonstrating that AMHs adapted to the rapid climate changes of the MIS 3 and could manage ecological risk, which would have played a major role in outcompeting Neanderthal populations.

We believe research design including site selection, choice of climate model, choice of model type (RF, logistic regression, etc.), the use of machine learning, and different research goals explain the differences between our modelling results and previously published material. As explained above, sites used in our models, while less numerous than for other published models, contain Aurignacian layers that can confidently be ascribed to interstadial or stadial periods (Paquin et al., 2023). The datasets produced are thus specifically curated to model the suitable habitat during both GI and GS conditions. Furthermore, the Random Forest algorithm is useful in making use of variables that have non-linear relationship with the dependent variable compared to general linear models (Genuer et al., 2010; Grömping, 2009) and a recent benchmark study confirms that it has good average prediction performance compared with other approaches (Couronné et al. 2018).

5 Conclusion

The predictive models produced in this research highlight variables that constituted suitable habitat for AMHs during cold and warm phases of MIS 3 and underline the impact of climate change and the importance of considering intra-annual climate variability.

623 Climate variables included in the models indicate that seasonal, rather than annual,
624 temperature and precipitation rates are important. Higher average temperatures in autumn
625 and less variability in spring precipitation rates would have been critical during GIs, while
626 less temperature variance in autumn and higher minimum monthly precipitation rates
627 during summer and autumn were critical during GSs.

628 Our results show that millennial-scale climate change and contrasting patterns of
629 climate variability affects the size of suitable habitat during stadial/interstadial events. The
630 timing and shape of the initial Aurignacian dispersal into Europe would have been
631 structured by millennial-scale climate change as a result. GSs display an irregular and
632 discontinuous suitable habitat across the two putative main routes of dispersal, the
633 Mediterranean coast and the Danube corridor, while GIs show a considerably more
634 extended and continuous suitable habitat along the coastal path. Our models agree with the
635 hypothesis that initial population dispersal into Europe was likely triggered by warm cycles
636 and their impacts on the environment (e.g., Badino et al., 2020; Müller et al., 2011),
637 probably around GI-12. The models also agree that the Danube valley West of the
638 Carpathians was a potential corridor of mobility throughout MIS 3, which agrees with
639 certain aspects of the *Kulturpumpe* hypothesis (Conard and Bolus, 2003).

640 The presence of climate variability predictors in the final models show that inter-
641 annual or seasonal variability also influenced human mobility during GIs and GSs, and that
642 ecological risk was therefore a significant factor governing dispersals. In this sense, the
643 low HS threshold observed during GSs can be interpreted as a mark of behavioral plasticity
644 on the part of early European populations which were able to deviate from their
645 environmental preferences and adapt to suboptimal climatic contexts in order to maintain

a larger vital space, which is coherent with the "generalist specialist" niche suggested by Roberts & Stewart (2018). It could also be taken to support the variability hypothesis of human evolution (Potts, 2013; Potts and Faith, 2015).

Supplementary Information

SI.1 – Modelling script (RF & GLM)

SI.2 – Modelling results (RF & GLM)

SI.3 – Variable correlation test and selection

SI.4 – Maps of each model

Data Availability

The archaeological data used in this study comes from a published database (Paquin et al., 2023) which can be downloaded at the following URL: http://www.hominindispersals.net/datasets

Acknowledgements

This work was supported by the Fonds de Recherche du Québec Société et Culture [2019-SE3-254686] and the Joseph-Armand Bombardier Canada Graduate Scholarships from the Social Sciences and Humanities Research Council of Canada [767-2017-1126]. Thanks are also due to Samuel Seuru and Catharina Igrejas Lopes Martins Costa for their precious help in the data compilation.

References

Albouy, B., Paquin, S., Hinz, M., Wren, C.D., Burke, A., 2023. The Last of Them: Investigating the Palaeogeography of the Last Neanderthals in Europe (Marine Isotopic Stage 3), in: Seuru, S., Albouy, B. (Eds.), Modelling Human-Environment Interactions in and beyond Prehistoric Europe, Themes in Contemporary Archaeology. Springer International Publishing, Cham, pp. 27–45. https://doi.org/10.1007/978-3-031-34336-0_2

Badino, F., Pini, R., Ravazzi, C., Margaritora, D., Arrighi, S., Bortolini, E., Figus, C., Giaccio, B., Lugli, F., Marciani, G., Monegato, G., Moroni, A., Negrino, F., Oxilia, G., Peresani, M., Romandini, M., Ronchitelli, A., Spinapolice, E.E., Zerboni, A., Benazzi, S., 2020. An overview of Alpine and Mediterranean palaeogeography, terrestrial ecosystems and climate history during MIS 3 with focus on the Middle to Upper Palaeolithic transition. Quat. Int., Peopling dynamics in the Mediterranean area between 45 and 39 ky ago: state of art and new data 551, 7–28. https://doi.org/10.1016/j.quaint.2019.09.024

Banks, W.E., d'Errico, F., Peterson, A.T., Kageyama, M., Sima, A., Sánchez-Goñi, M.-F., 2008. Neanderthal Extinction by Competitive Exclusion. PLoS ONE 3, e3972. https://doi.org/10.1371/journal.pone.0003972

Banks, W.E., d'Errico, F., Zilhão, J., 2013a. Human–climate interaction during the Early Upper Paleolithic: testing the hypothesis of an adaptive shift between the Proto-Aurignacian and the Early Aurignacian. J. Hum. Evol. 64, 39–55. https://doi.org/10.1016/j.jhevol.2012.10.001

686 Banks, W.E., d'Errico, F., Zilhão, J., 2013b. Revisiting the chronology of the Proto-
687 Aurignacian and the Early Aurignacian in Europe: A reply to Higham et al.'s
688 comments on Banks et al. (2013). J. Hum. Evol. 65, 810–817.
689 https://doi.org/10.1016/j.jhevol.2013.08.004

690 Barbet-Massin, M., Jiguet, F., Albert, C.H., Thuiller, W., 2012. Selecting pseudo-
691 absences for species distribution models: how, where and how many? Methods
692 Ecol. Evol. 3, 327–338. https://doi.org/10.1111/j.2041-210X.2011.00172.x

693 Barshay-Szmidt, C., Normand, C., Flas, D., Soulier, M.-C., 2018. Radiocarbon dating the
694 Aurignacian sequence at Isturitz (France): Implications for the timing and
695 development of the Protoaurignacian and Early Aurignacian in western Europe. J.
696 Archaeol. Sci. Rep. 17, 809–838. https://doi.org/10.1016/j.jasrep.2017.09.003

697 Bataille, G., Tafelmaier, Y., Weniger, G.-C., 2018. Living on the edge – A comparative
698 approach for studying the beginning of the Aurignacian. Quat. Int.,
699 Chronostratigraphic data about the Middle to Upper Palaeolithic cultural change
700 in Iberian Peninsula 474, 3–29. https://doi.org/10.1016/j.quaint.2018.03.024

701 Benazzi, S., Slon, V., Talamo, S., Negrino, F., Peresani, M., Bailey, S.E., Sawyer, S.,
702 Panetta, D., Vicino, G., Starnini, E., Mannino, M.A., Salvadori, P.A., Meyer, M.,
703 Pääbo, S., Hublin, J.-J., 2015. The makers of the Protoaurignacian and
704 implications for Neandertal extinction. Science 348, 793–796.
705 https://doi.org/10.1126/science.aaa2773

706 Breiman, L., 2001. Random Forests. Mach. Learn. 45, 5–32.
707 https://doi.org/10.1023/A:1010933404324

Burke, A., Kageyama, M., Latombe, G., Fasel, M., Vrac, M., Ramstein, G., James, P.M.A., 2017. Risky business: The impact of climate and climate variability on human population dynamics in Western Europe during the Last Glacial Maximum. Quat. Sci. Rev. 164, 217–229. https://doi.org/10.1016/j.quascirev.2017.04.001

Burke, A., Levavasseur, G., James, P.M.A., Guiducci, D., Izquierdo, M.A., Bourgeon, L., Kageyama, M., Ramstein, G., Vrac, M., 2014. Exploring the impact of climate variability during the Last Glacial Maximum on the pattern of human occupation of Iberia. J. Hum. Evol. 73, 35–46. https://doi.org/10.1016/j.jhevol.2014.06.003

Carto, S.L., Weaver, A.J., Hetherington, R., Lam, Y., Wiebe, E.C., 2009. Out of Africa and into an ice age: on the role of global climate change in the late Pleistocene migration of early modern humans out of Africa. J. Hum. Evol. 56, 139–151. https://doi.org/10.1016/j.jhevol.2008.09.004

Conard, N.J., Bolus, M., 2003. Radiocarbon dating the appearance of modern humans and timing of cultural innovations in Europe: new results and new challenges. J. Hum. Evol. 44, 331–371. https://doi.org/10.1016/S0047-2484(02)00202-6

Couronné, R., Probst, P., Boulesteix, A.-L., 2018. Random forest versus logistic regression: a large-scale benchmark experiment. BMC Bioinformatics 19, 270. https://doi.org/10.1186/s12859-018-2264-5

d'Errico, F., Sánchez Goñi, M.F., 2003. Neandertal extinction and the millennial scale climatic variability of OIS 3. Quat. Sci. Rev. 22, 769–788. https://doi.org/10.1016/S0277-3791(03)00009-X

d'Errico, F., Zilhão, J., Julien, M., Baffier, D., Pelegrin, J., 1998. Neanderthal Acculturation in Western Europe? A Critical Review of the Evidence and Its Interpretation. Curr. Anthropol. 39, S1–S44. https://doi.org/10.1086/204689

Dansgaard, W., Clausen, H.B., Gundestrup, N., Hammer, C.U., Johnsen, S.F., Kristinsdottir, P.M., Reeh, N., 1982. A New Greenland Deep Ice Core. Science 218, 1273–1277. https://doi.org/10.1126/science.218.4579.1273

Davies, W., 2007. Re-evaluating the Aurignacian as an Expression of Modern Human Mobility and Dispersal, in: Rethinking the Human Revolution. pp. 263–274.

Davies, W., 2001. A Very Model of a Modern Human Industry: New Perspectives on the Origins and Spread of the Aurignacian in Europe. Proc. Prehist. Soc. 67, 195–217. https://doi.org/10.1017/S0079497X00001663

Davies, W., Gollop, P., 2003. The Human Presence in Europe during the Last Glacial Period II: Climate Tolerance and Climate Preferences of Mid-and Late Glacial Hominids, in: Van Andel, T.H., Davies, W., Aiello, L. (Eds.), Neanderthals and Modern Humans in the European Landscape during the Last Glaciation : Archaeological Results of the Stage 3 Project. McDonald Institute for Archaeological Research, pp. 131–146.

Díaz-Uriarte, R., Alvarez de Andrés, S., 2006. Gene selection and classification of microarray data using random forest. BMC Bioinformatics 7, 3. https://doi.org/10.1186/1471-2105-7-3

Dinnis, R., 2012. The archaeology of Britain&s first modern humans. Antiquity 86, 627–641. https://doi.org/10.1017/S0003598X00047815

752 Dufresne, J.-L., Foujols, M.-A., Denvil, S., Caubel, A., Marti, O., Aumont, O., Balkanski,
753 Y., Bekki, S., Bellenger, H., Benshila, R., Bony, S., Bopp, L., Braconnot, P.,
754 Brockmann, P., Cadule, P., Cheruy, F., Codron, F., Cozic, A., Cugnet, D., de
755 Noblet, N., Duvel, J.-P., Ethé, C., Fairhead, L., Fichefet, T., Flavoni, S.,
756 Friedlingstein, P., Grandpeix, J.-Y., Guez, L., Guilyardi, E., Hauglustaine, D.,
757 Hourdin, F., Idelkadi, A., Ghattas, J., Joussaume, S., Kageyama, M., Krinner, G.,
758 Labetoulle, S., Lahellec, A., Lefebvre, M.-P., Lefevre, F., Levy, C., Li, Z.X.,
759 Lloyd, J., Lott, F., Madec, G., Mancip, M., Marchand, M., Masson, S.,
760 Meurdesoif, Y., Mignot, J., Musat, I., Parouty, S., Polcher, J., Rio, C., Schulz, M.,
761 Swingedouw, D., Szopa, S., Talandier, C., Terray, P., Viovy, N., Vuichard, N.,
762 2013. Climate change projections using the IPSL-CM5 Earth System Model: from
763 CMIP3 to CMIP5. Clim. Dyn. 40, 2123–2165. https://doi.org/10.1007/s00382-
764 012-1636-1

765 Ehlers, J., Gibbard, P.L., Hughes, P.D. (Eds.), 2011. Quaternary glaciations - extent and
766 chronology: a closer look, Developments in Quaternary science. Elsevier,
767 Amsterdam ; Boston.

768 Falcucci, A., Conard, N.J., Peresani, M., 2017. A critical assessment of the
769 Protoaurignacian lithic technology at Fumane Cave and its implications for the
770 definition of the earliest Aurignacian. PLOS ONE 12, e0189241.
771 https://doi.org/10.1371/journal.pone.0189241

772 Fasel, M., 2014. STI: Calculation offthe Standardized Temperature Index. R Package
773 version 01.

774 Floss, H., Fröhle, S., Wettengl, S., 2016. The Aurignacian along the Danube. Its Two-

775 Fold Role as a Transalpine and Cisalpine Passageway of Early Homo Sapiens into
776 Europe, in: Krauss, R., Floss, H. (Eds.), Southeast Europe Before Neolithisation -
777 Proceedings of the International Workshop within the Collaborative Research
778 Centres Sfb 1070 “RessourcenKulturen”, Schloss Hohentübingen, 9th of May
779 2014. Universität Tübingen.

780 Formicola, V., 1989. Early Aurignatian Deciduous Incisor from Riparo Bombrini at Balzi
781 Rossi (Grimaldi, Italy). Riv. Antropol. 67, 287–292.

782 Gamble, C., Davies, W., Pettitt, P., Richards, M., 2004. Climate change and evolving
783 human diversity in Europe during the last glacial. Philos. Trans. R. Soc. B Biol.
784 Sci. 359, 243–254. https://doi.org/10.1098/rstb.2003.1396

785 Genuer, R., Poggi, J.-M., Tuleau-Malot, C., 2010. Variable selection using random
786 forests. Pattern Recognit. Lett. 31, 2225–2236.
787 https://doi.org/10.1016/j.patrec.2010.03.014

788 Grömping, U., 2009. Variable Importance Assessment in Regression: Linear Regression
789 versus Random Forest. Am. Stat. 63, 308–319.
790 https://doi.org/10.1198/tast.2009.08199

791 Guttman, N.B., 1999. Accepting the Standardized Precipitation Index: A Calculation
792 Algorithm1. JAWRA J. Am. Water Resour. Assoc. 35, 311–322.
793 https://doi.org/10.1111/j.1752-1688.1999.tb03592.x

794 Hauck, T.C., Lehmkuhl, F., Zeeden, C., Bösken, J., Thiemann, A., Richter, J., 2018. The
795 Aurignacian way of life: Contextualizing early modern human adaptation in the
796 Carpathian Basin. Quat. Int. 485, 150–166.

https://doi.org/10.1016/j.quaint.2017.10.020

Haws, J.A., Benedetti, M.M., Talamo, S., Bicho, N., Cascalheira, J., Ellis, M.G., Carvalho, M.M., Friedl, L., Pereira, T., Zinsious, B.K., 2020. The early Aurignacian dispersal of modern humans into westernmost Eurasia. Proc. Natl. Acad. Sci. 117, 25414–25422. https://doi.org/10.1073/pnas.2016062117

Hayes, M.J., 2000. Revisiting the SPI: Clarifying the Process. Drought Netw. News 1994-2001 18.

Hershkovitz, I., Weber, G.W., Quam, R., Duval, M., Grün, R., Kinsley, L., Ayalon, A., Bar-Matthews, M., Valladas, H., Mercier, N., Arsuaga, J.L., Martinón-Torres, M., Bermúdez de Castro, J.M., Fornai, C., Martín-Francés, L., Sarig, R., May, H., Krenn, V.A., Slon, V., Rodríguez, L., García, R., Lorenzo, C., Carretero, J.M., Frumkin, A., Shahack-Gross, R., Bar-Yosef Mayer, D.E., Cui, Y., Wu, X., Peled, N., Groman-Yaroslavski, I., Weissbrod, L., Yeshurun, R., Tsatskin, A., Zaidner, Y., Weinstein-Evron, M., 2018. The earliest modern humans outside Africa. Science 359, 456–459. https://doi.org/10.1126/science.aap8369

Higham, T., Douka, K., Wood, R., Ramsey, C.B., Brock, F., Basell, L., Camps, M., Arrizabalaga, A., Baena, J., Barroso-Ruíz, C., Bergman, C., Boitard, C., Boscato, P., Caparrós, M., Conard, N.J., Draily, C., Froment, A., Galván, B., Gambassini, P., Garcia-Moreno, A., Grimaldi, S., Haesaerts, P., Holt, B., Iriarte-Chiapusso, M.-J., Jelinek, A., Jordá Pardo, J.F., Maíllo-Fernández, J.-M., Marom, A., Maroto, J., Menéndez, M., Metz, L., Morin, E., Moroni, A., Negrino, F., Panagopoulou, E., Peresani, M., Pirson, S., de la Rasilla, M., Riel-Salvatore, J., Ronchitelli, A., Santamaria, D., Semal, P., Slimak, L., Soler, J., Soler, N., Villaluenga, A.,

Pinhasi, R., Jacobi, R., 2014. The timing and spatiotemporal patterning of Neanderthal disappearance. Nature 512, 306–309. https://doi.org/10.1038/nature13621

Hinguant, S., Monnier, J.-L., 2013. Le Paléolithique supérieur ancien dans le Massif armoricain : un état de la question, in: Bodu, P., Chehmana, L., Klaric, L., Mevel, L., Soriano, S., Teyssandier, N. (Eds.), Le Paléolithique Supérieur Ancien de l'Europe Du Nord-Ouest : Réflexions et Synthèses à Partir d'un Projet Collectif de Recherche Sur Le Centre et Le Sud Du Bassin Parisien - Actes Du Colloque de Sens (15-18 Avril 2009), Mémoires de La Société Préhistorique Française. pp. 229–238.

Hublin, J.-J., 2015. The modern human colonization of western Eurasia: when and where? Quat. Sci. Rev., Synchronising Environmental and Archaeological Records using Volcanic Ash Isochrons 118, 194–210. https://doi.org/10.1016/j.quascirev.2014.08.011

Jones, J.R., Richards, M.P., Reade, H., Bernaldo de Quirós, F., Marín-Arroyo, A.B., 2019. Multi-Isotope investigations of ungulate bones and teeth from El Castillo and Covalejos caves (Cantabria, Spain): Implications for paleoenvironment reconstructions across the Middle-Upper Palaeolithic transition. J. Archaeol. Sci. Rep. 23, 1029–1042. https://doi.org/10.1016/j.jasrep.2018.04.014

Kelly, R.L., 2013. The Lifeways of Hunter-Gatherers: The Foraging Spectrum. Cambridge University Press. Archaeol Anthropol Sci 8, 779–803. https://doi.org/10.1007/s12520-015-0253-4

842 Kim, Y., Kimball, J.S., Didan, K., Henebry, G.M., 2014. Response of vegetation growth
843 and productivity to spring climate indicators in the conterminous United States
844 derived from satellite remote sensing data fusion. Agric. For. Meteorol. 194, 132–
845 143. https://doi.org/10.1016/j.agrformet.2014.04.001

846 Klein, K., Wegener, C., Schmidt, I., Rostami, M., Ludwig, P., Ulbrich, S., Richter, J.,
847 Weniger, G.-C., Shao, Y., 2021. Human existence potential in Europe during the
848 Last Glacial Maximum. Quat. Int. 581–582, 7–27.
849 https://doi.org/10.1016/j.quaint.2020.07.046

850 Klein, K., Weniger, G.-C., Ludwig, P., Stepanek, C., Zhang, X., Wegener, C., Shao, Y.,
851 2023. Assessing climatic impact on transition from Neanderthal to anatomically
852 modern human population on Iberian Peninsula: a macroscopic perspective. Sci.
853 Bull. 68, 1176–1186. https://doi.org/10.1016/j.scib.2023.04.025

854 Latombe, G., Burke, A., Vrac, M., Levavasseur, G., Dumas, C., Kageyama, M.,
855 Ramstein, G., 2018. Comparison of spatial downscaling methods of general
856 circulation model results to study climate variability during the Last Glacial
857 Maximum. Geosci. Model Dev. 11, 2563–2579. https://doi.org/10.5194/gmd-11-
858 2563-2018

859 Le Mézo, P., Beaufort, L., Bopp, L., Braconnot, P., Kageyama, M., 2017. From monsoon
860 to marine productivity in the Arabian Sea: insights from glacial and interglacial
861 climates. Clim. Past 13, 759–778. https://doi.org/10.5194/cp-13-759-2017

862 Lézine, A.-M., Kageyama, M., Bassinot, F., 2023. Data and models reveal humid
863 environmental conditions during MIS 3 in two of the world's largest deserts.

Comptes Rendus Geosci. 355, 229–246. https://doi.org/10.5802/crgeos.240

Ludwig, P., Shao, Y., Kehl, M., Weniger, G.-C., 2018. The Last Glacial Maximum and Heinrich event I on the Iberian Peninsula: A regional climate modelling study for understanding human settlement patterns. Glob. Planet. Change 170, 34–47. https://doi.org/10.1016/j.gloplacha.2018.08.006

Maier, A., Lehmkuhl, F., Ludwig, P., Melles, M., Schmidt, I., Shao, Y., Zeeden, C., Zimmermann, A., 2016. Demographic estimates of hunter–gatherers during the Last Glacial Maximum in Europe against the background of palaeoenvironmental data. Quat. Int. 425, 49–61. https://doi.org/10.1016/j.quaint.2016.04.009

Malmierca-Vallet, I., Sime, L.C., the D–O community members, 2023. Dansgaard–Oeschger events in climate models: review and baseline Marine Isotope Stage 3 (MIS3) protocol. Clim. Past 19, 915–942. https://doi.org/10.5194/cp-19-915-2023

McKee, T.D., Doesken, N.J., Kleist, J., 1993. The relationship of drought frequency and duration to time scales., in: Proceedings of the 8th Conference of Applied Climatology. American Meterological Society, Anaheim, California, pp. 179–184.

Mellars, P., 2006. A new radiocarbon revolution and the dispersal of modern humans in Eurasia. Nature 439, 931–935. https://doi.org/10.1038/nature04521

Mellars, P., 2011. The earliest modern humans in Europe. Nature 479, 483–485. https://doi.org/10.1038/479483a

Müller, U.C., Pross, J., Tzedakis, P.C., Gamble, C., Kotthoff, U., Schmiedl, G., Wulf, S., Christanis, K., 2011. The role of climate in the spread of modern humans into

886 Europe. Quat. Sci. Rev. 30, 273–279.
887 https://doi.org/10.1016/j.quascirev.2010.11.016

888 Paquin, S., Albouy, B., Hinz, M., Burke, A., 2023. Going New Places: Dispersal and
889 Establishment of the Aurignacian Technocomplex in Europe During the Marine
890 Isotopic Stage 3 (MIS 3), in: Seuru, S., Albouy, B. (Eds.), Modelling Human-
891 Environment Interactions in and beyond Prehistoric Europe, Themes in
892 Contemporary Archaeology. Springer International Publishing, Cham, pp. 47–59.
893 https://doi.org/10.1007/978-3-031-34336-0_3

894 Peltier, W.R., Argus, D.F., Drummond, R., 2015. Space geodesy constrains ice age
895 terminal deglaciation: The global ICE-6G_C (VM5a) model. J. Geophys. Res.
896 Solid Earth 120, 450–487. https://doi.org/10.1002/2014JB011176

897 Posth, C., Yu, H., Ghalichi, A., Rougier, H., Crevecoeur, I., Huang, Y., Ringbauer, H.,
898 Rohrlach, A.B., Nägele, K., Villalba-Mouco, V., Radzeviciute, R., Ferraz, T.,
899 Stoessel, A., Tukhbatova, R., Drucker, D.G., Lari, M., Modi, A., Vai, S., Saupe,
900 T., Scheib, C.L., Catalano, G., Pagani, L., Talamo, S., Fewlass, H., Klaric, L.,
901 Morala, A., Rué, M., Madelaine, S., Crépin, L., Caverne, J.-B., Bocaege, E.,
902 Ricci, S., Boschin, F., Bayle, P., Maureille, B., Le Brun-Ricalens, F., Bordes, J.-
903 G., Oxilia, G., Bortolini, E., Bignon-Lau, O., Debout, G., Orliac, M., Zazzo, A.,
904 Sparacello, V., Starnini, E., Sineo, L., van der Plicht, J., Pecqueur, L., Merceron,
905 G., Garcia, G., Leuvrey, J.-M., Garcia, C.B., Gómez-Olivencia, A., Połtowicz-
906 Bobak, M., Bobak, D., Le Luyer, M., Storm, P., Hoffmann, C., Kabaciński, J.,
907 Filimonova, T., Shnaider, S., Berezina, N., González-Rabanal, B., González
908 Morales, M.R., Marín-Arroyo, A.B., López, B., Alonso-Llamazares, C.,

Ronchitelli, A., Polet, C., Jadin, I., Cauwe, N., Soler, J., Coromina, N., Rufí, I., Cottiaux, R., Clark, G., Straus, L.G., Julien, M.-A., Renhart, S., Talaa, D., Benazzi, S., Romandini, M., Amkreutz, L., Bocherens, H., Wißing, C., Villotte, S., de Pablo, J.F.-L., Gómez-Puche, M., Esquembre-Bebia, M.A., Bodu, P., Smits, L., Souffi, B., Jankauskas, R., Kozakaitė, J., Cupillard, C., Benthien, H., Wehrberger, K., Schmitz, R.W., Feine, S.C., Schüler, T., Thevenet, C., Grigorescu, D., Lüth, F., Kotula, A., Piezonka, H., Schopper, F., Svoboda, J., Sázelová, S., Chizhevsky, A., Khokhlov, A., Conard, N.J., Valentin, F., Harvati, K., Semal, P., Jungklaus, B., Suvorov, A., Schulting, R., Moiseyev, V., Mannermaa, K., Buzhilova, A., Terberger, T., Caramelli, D., Altena, E., Haak, W., Krause, J., 2023. Palaeogenomics of Upper Palaeolithic to Neolithic European hunter-gatherers. Nature 615, 117–126. https://doi.org/10.1038/s41586-023-05726-0

Potts, R., 2013. Hominin evolution in settings of strong environmental variability. Quat. Sci. Rev. 73, 1–13. https://doi.org/10.1016/j.quascirev.2013.04.003

Potts, R., Faith, J.T., 2015. Alternating high and low climate variability: The context of natural selection and speciation in Plio-Pleistocene hominin evolution. J. Hum. Evol. 87, 5–20. https://doi.org/10.1016/j.jhevol.2015.06.014

R Core Team, 2023. R: A Language and Environment for Statistical Computing.

Rasmussen, S.O., Bigler, M., Blockley, S.P., Blunier, T., Buchardt, S.L., Clausen, H.B., Cvijanovic, I., Dahl-Jensen, D., Johnsen, S.J., Fischer, H., Gkinis, V., Guillevic, M., Hoek, W.Z., Lowe, J.J., Pedro, J.B., Popp, T., Seierstad, I.K., Steffensen, J.P., Svensson, A.M., Vallelonga, P., Vinther, B.M., Walker, M.J.C., Wheatley, J.J.,

Winstrup, M., 2014. A stratigraphic framework for abrupt climatic changes during the Last Glacial period based on three synchronized Greenland ice-core records: refining and extending the INTIMATE event stratigraphy. Quat. Sci. Rev., Dating, Synthesis, and Interpretation of Palaeoclimatic Records and Model-data Integration: Advances of the INTIMATE project(INTegration of Ice core, Marine and TErrestrial records, COST Action ES0907) 106, 14–28. https://doi.org/10.1016/j.quascirev.2014.09.007

Riel-Salvatore, J., Negrino, F., 2018. Proto-Aurignacian Lithic Technology, Mobility, and Human Niche Construction: A Case Study from Riparo Bombrini, Italy, in: Robinson, E., Sellet, F. (Eds.), Lithic Technological Organization and Paleoenvironmental Change: Global and Diachronic Perspectives, Studies in Human Ecology and Adaptation. Springer International Publishing, Cham, pp. 163–187. https://doi.org/10.1007/978-3-319-64407-3_8

Roberts, P., Stewart, B.A., 2018. Defining the 'generalist specialist' niche for Pleistocene Homo sapiens. Nat. Hum. Behav. 2, 542–550. https://doi.org/10.1038/s41562-018-0394-4

Schmidt, I., Bradtmöller, M., Kehl, M., Pastoors, A., Tafelmaier, Y., Weninger, B., Weniger, G.-C., 2012. Rapid climate change and variability of settlement patterns in Iberia during the Late Pleistocene. Quat. Int., Temporal and spatial corridors of Homo sapiens sapiens population dynamics during the Late Pleistocene and Early Holocene 274, 179–204. https://doi.org/10.1016/j.quaint.2012.01.018

Shao, Y., Limberg, H., Klein, K., Wegener, C., Schmidt, I., Weniger, G.-C., Hense, A., Rostami, M., 2021. Human-existence probability of the Aurignacian techno-

complex under extreme climate conditions. Quat. Sci. Rev. 263, 106995. https://doi.org/10.1016/j.quascirev.2021.106995

Slimak, L., Zanolli, C., Higham, T., Frouin, M., Schwenninger, J.-L., Arnold, L.J., Demuro, M., Douka, K., Mercier, N., Guérin, G., Valladas, H., Yvorra, P., Giraud, Y., Seguin-Orlando, A., Orlando, L., Lewis, J.E., Muth, X., Camus, H., Vandevelde, S., Buckley, M., Mallol, C., Stringer, C., Metz, L., 2022. Modern human incursion into Neanderthal territories 54,000 years ago at Mandrin, France. Sci. Adv. 8, eabj9496. https://doi.org/10.1126/sciadv.abj9496

Sterling, K., 2015. Black Feminist Theory in Prehistory. Archaeologies 11, 93–120. https://doi.org/10.1007/s11759-015-9265-z

Tallavaara, M., Luoto, M., Korhonen, N., Järvinen, H., Seppä, H., 2015. Human population dynamics in Europe over the Last Glacial Maximum. Proc. Natl. Acad. Sci. 112, 8232–8237. https://doi.org/10.1073/pnas.1503784112

Timmermann, A., 2020. Quantifying the potential causes of Neanderthal extinction: Abrupt climate change versus competition and interbreeding. Quat. Sci. Rev. 238, 106331. https://doi.org/10.1016/j.quascirev.2020.106331

Timmermann, A., Yun, K.-S., Raia, P., Ruan, J., Mondanaro, A., Zeller, E., Zollikofer, C., Ponce de León, M., Lemmon, D., Willeit, M., Ganopolski, A., 2022. Climate effects on archaic human habitats and species successions. Nature 604, 495–501. https://doi.org/10.1038/s41586-022-04600-9

Tsakanikou, P., McNabb, J., 2023. Refloating the Aegean Lost Dryland: An Affordance-Based GIS Approach to Explore the Interaction Between Hominins and the

977 Palaeolandscape, in: Seuru, S., Albouy, B. (Eds.), Modelling Human-
978 Environment Interactions in and beyond Prehistoric Europe, Themes in
979 Contemporary Archaeology. Springer International Publishing, Cham, pp. 3–26.
980 https://doi.org/10.1007/978-3-031-34336-0_1

981 Tzedakis, P.C., Hughen, K.A., Cacho, I., Harvati, K., 2007. Placing late Neanderthals in a
982 climatic context. Nature 449, 206–208. https://doi.org/10.1038/nature06117

983 Vaks, A., Bar-Matthews, M., Ayalon, A., Matthews, A., Halicz, L., Frumkin, A., 2007.
984 Desert speleothems reveal climatic window for African exodus of early modern
985 humans. Geology 35, 831–834. https://doi.org/10.1130/G23794A.1

986 Van Andel, T.H., Davies, W., weniger, B., 2003. The Human Presence in Europe during
987 the Last Glacial Period I: Human Migrations and the Changing Climate, in: Van
988 Andel, T.H., Davies, W., Aiello, L. (Eds.), Neanderthals and Modern Humans in
989 the European Landscape during the Last Glaciation : Archaeological Results of
990 the Stage 3 Project. McDonald Institute for Archaeological Research, pp. 31–56.

991 Vicente-Serrano, S.M., Beguería, S., López-Moreno, J.I., 2010. A Multiscalar Drought
992 Index Sensitive to Global Warming: The Standardized Precipitation
993 Evapotranspiration Index. J. Clim. 23, 1696–1718.
994 https://doi.org/10.1175/2009JCLI2909.1

995 Vidal-Cordasco, M., Ocio, D., Hickler, T., Marín-Arroyo, A.B., 2022. Ecosystem
996 productivity affected the spatiotemporal disappearance of Neanderthals in Iberia.
997 Nat Ecol Evol 6, 1644–1657. https://doi.org/10.1038/s41559-022-01861-5

998 Villa, P., Pollarolo, L., Conforti, J., Marra, F., Biagioni, C., Degano, I., Lucejko, J.J.,

Tozzi, C., Pennacchioni, M., Zanchetta, G., Nicosia, C., Martini, M., Sibilia, E., Panzeri, L., 2018. From Neandertals to modern humans: New data on the Uluzzian. PLOS ONE 13, e0196786. https://doi.org/10.1371/journal.pone.0196786

Villaverde, V., Sanchis, A., Badal, E., Bel, M.Á., Bergadà, M.M., Eixea, A., Guillem, P.M., Martínez-Alfaro, Á., Martínez-Valle, R., Martínez-Varea, C.M., Real, C., Steier, P., Wild, E.M., 2021. Cova de les Malladetes (Valencia, Spain): New Insights About the Early Upper Palaeolithic in the Mediterranean Basin of the Iberian Peninsula. J. Paleolit. Archaeol. 4, 5. https://doi.org/10.1007/s41982-021-00081-w

Vrac, M., Marbaix, P., Paillard, D., Naveau, P., 2007. Non-linear statistical downscaling of present and LGM precipitation and temperatures over Europe. Clim. Past 3, 669–682. https://doi.org/10.5194/cp-3-669-2007

Weniger, G.-C., de Andrés-Herrero, M., Bolin, V., Kehl, M., Otto, T., Potì, A., Tafelmaier, Y., 2019. Late Glacial rapid climate change and human response in the Westernmost Mediterranean (Iberia and Morocco). PLOS ONE 14, e0225049. https://doi.org/10.1371/journal.pone.0225049

Winterhalder, B., Lu, F., Tucker, B., 1999. Risk-senstive adaptive tactics: Models and evidence from subsistence studies in biology and anthropology. J. Archaeol. Res. 7, 301–348. https://doi.org/10.1007/BF02446047

Wisz, M.S., Guisan, A., 2009. Do pseudo-absence selection strategies influence species distribution models and their predictions? An information-theoretic approach

based on simulated data. BMC Ecol. 9, 8. https://doi.org/10.1186/1472-6785-9-8

Woillez, M.-N., Levavasseur, G., Daniau, A.-L., Kageyama, M., Urrego, D.H., Sánchez-Goñi, M.-F., Hanquiez, V., 2014. Impact of precession on the climate, vegetation and fire activity in southern Africa during MIS4. Clim. Past 10, 1165–1182. https://doi.org/10.5194/cp-10-1165-2014

Wren, C.D., Burke, A., 2019. Habitat suitability and the genetic structure of human populations during the Last Glacial Maximum (LGM) in Western Europe. PLOS ONE 14, e0217996. https://doi.org/10.1371/journal.pone.0217996

Yravedra-Sainz de los Terreros, J., Gómez-Castanedo, A., Aramendi-Picado, J., Montes-Barquín, R., Sanguino-González, J. 2016. Neanderthal and Homo sapiens subsistence strategies in the Cantabrian region of northern Spain. Archaeol Anthropol Sci 8, 779–803. https://doi.org/10.1007/s12520-015-0253-4

Zapata, M.B.R., García, M.J.G., 2005. Los neandertales cantábricos: su paisaje vegetal, in: Neandertales Cantábricos, Estado de La Cuestión: Actas de La Reunión Científica: Celebrada En El Museo de Altamira Los Días 20-22 de Octubre de 2004. Subdirección General de Publicaciones, Información y Documentación, pp. 275–284.

Zilhão, J., 2021. The late persistence of the Middle Palaeolithic and Neandertals in Iberia: A review of the evidence for and against the “Ebro Frontier” model. Quat. Sci. Rev. 270, 107098. https://doi.org/10.1016/j.quascirev.2021.107098

Zilhão, J., 2000. The Ebro frontier: a model for the late extinction of Iberian Neanderthals, in: Finlayson, C. (Ed.), Neanderthals on the Edge: 150th

Anniversary Conference of the Forbes' Quarry Discovery. Gibraltar, pp. 111–121.

Zilhão, J., d'Errico, F., 1999. The Chronology and Taphonomy of the Earliest Aurignacian and Its Implications for the Understanding of Neandertal Extinction. J. World Prehistory 13, 1–68.